Complex Implications of Translational Invariance in Polymer Field Theory

Jaeup U. Kim, †,‡ Mark W. Matsen, *,‡,¶,§ David C. Morse, $^{*,\parallel}$ and James D. Willis \P

†Department of Physics, Ulsan National Institute of Science and Technology (UNIST),
Ulsan 44919, Republic of Korea

‡Department of Chemical Engineering, University of Waterloo, 200 University Ave. W.,
Waterloo, Ontario N2L 3G1, Canada

¶Department of Physics & Astronomy, University of Waterloo, 200 University Ave. W.,

Waterloo, Ontario N2L 3G1, Canada

§ Waterloo Institute of Nanotechnology, University of Waterloo, 200 University Ave. W.,
Waterloo, Ontario N2L 3G1, Canada

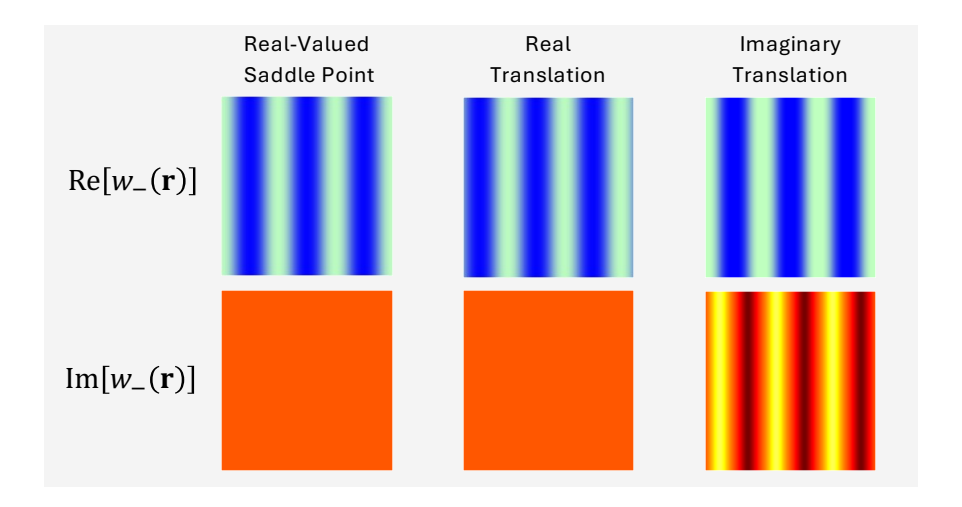
|| Department of Chemical Engineering & Materials Science, University of Minnesota, 421

Washington Ave. S.E., Minneapolis, MN 55455, USA

E-mail: mwmatsen@uwaterloo.ca; morse012@umn.edu

Abstract

The behavior of complex-Langevin field-theoretic simulations (CL-FTSs) of polymer liquids is sensitive to the nature of saddle-point field configurations, which are solutions of self-consistent field theory (SCFT). Recent work [Kang et al. *Macromolecules* **2024**, *57*, 3850] has shown that SCFT saddle-points with real fields are generally not isolated solutions but rather members of a low-dimensional family of continuously-connected complex-valued saddle-points sharing the same Hamiltonian value. We show that this behavior is a natural consequence of the analyticity and translational invariance of the Hamiltonian, which together demand its invariance under generalized translations by displacements with complex components. We also present a numerical algorithm that minimizes the deleterious effects of this generalized symmetry on the stability of CL-FTSs.



For Table of Contents Use Only

Introduction

Several different types of polymer field theory play important roles in the study of polymeric materials. The theories of interest here all relate the free energy of an interacting liquid to the properties of a hypothetical gas of non-interacting polymers subjected to inhomogeneous chemical potentials, referred to as fields, w. In self-consistent field theory (SCFT), $^{1-3}$ an inhomogeneous structure (or phase) is represented by the field configuration corresponding to a saddle-point of the associated Hamiltonian functional, H[w]. Field-theoretic simulation (FTS) methods, $^{3-5}$ on the other hand, sample an ensemble of fluctuating fields, and they are able to handle complicated systems $^{6-11}$ that are beyond the capabilities of conventional particle-based simulations.

FTS methods are based on an exact transformation of the partition function from an integral over particle coordinates into a functional integral over fields. However, this transformation leads to a complex-valued H[w], and thus to a complex generalized Boltzmann weight, $P_c[w] = \exp(-H[w]/k_BT)$. Straightforward methods of sampling the resulting distribution are susceptible to a severe 'sign problem' arising from rapid fluctuations in both the real and imaginary components of $P_c[w]$. This sign problem can be effectively addressed by adopting the complex-Langevin field-theoretic simulation (CL-FTS) method, ¹² in which the fields are permitted to explore the entire complex domain and $P_c[w]$ is replaced by a nonnegative real-valued weight, P[w]. Provided a CL-FTS reaches a steady state, the resulting ensemble averages should be equivalent to those of the original model.⁵

The field-theoretic Hamiltonian for a polymeric system is typically expressed as

$$H[w] = -k_B T \ln Z_{id}[w] + H_f[w]$$
(1)

where $H_f[w]$ is a simple quadratic functional of the fields and $Z_{id}[w]$ is the partition function of a hypothetical ideal gas of non-interacting polymers in which monomers of type i at position \mathbf{r} are subjected to a fluctuating complex field, $w_i(\mathbf{r})$. A CL-FTS can be performed in either a canonical or grand-canonical statistical ensemble by simply evaluating $Z_{id}[w]$ in the same ensemble. In systems involving two monomer species, labeled A and B, the Hamiltonian is a functional of two 'species' fields, $w_A(\mathbf{r})$ and $w_B(\mathbf{r})$. For convenience, however, H[w] is generally expressed as a functional of two 'exchange' fields, defined as $w_{\pm}(\mathbf{r}) = [w_A(\mathbf{r}) \pm w_B(\mathbf{r})]/2$. Supporting Information presents explicit expressions for the Hamiltonian of a diblock copolymer melt, as well as a detailed discussion of the analytic properties of $P_c[w]$ and H[w].

When applied to a liquid of long chains, with a large invariant degree of polymerization \bar{N} , the fields of a CL-FTS generally fluctuate about saddle-point configurations. Until recently, it has generally been assumed that the relevant saddle-points in CL-FTSs are the usual ones of SCFT involving real-valued monomer species fields. We hereafter refer to these as the real-valued or real saddle-points. Furthermore, it has been assumed that these saddle-points (also referred to as 'physical' saddle-points) are isolated from all other saddle-points. ¹⁴

The assumption that the saddle-points are real-valued and isolated was recently shown to be false by Kang, Yong, and Kim (KYK). 15 They found that each real-valued saddle-point is instead a member of a low-dimensional space of continuously-connected complex-valued saddle-points that share a common real value of H[w]. As one analytically tractable example, KYK derived a family of complex saddle-points for an interface separating semi-infinite phases of immiscible A and B homopolymers in the strong-segregation limit. In particular, they generalized the real-valued solution obtained by Helfand and Tagami (HT), 16,17 and showed that it is part of a family of complex-valued saddle-points all corresponding to the same real value of the Hamiltonian. KYK also presented numerical evidence for the existence of analogous sets of complex saddle-points associated with SCFT solutions for the lamellar, cylindrical, bcc spherical, and double-gyroid phases of diblock copolymer melts. Again, each set of complex-valued saddle-points included the usual real-valued saddle-point as a special case and exhibited the same real value for the Hamiltonian. Here, we provide a fundamental explanation for this discovery by KYK.

Generalized Translations

The observed invariance of H[w] within each infinite set of saddle-points suggests that their field configurations are related by an underlying symmetry. Furthermore, a strong clue to the nature of this symmetry is provided by the complex-valued solution derived by KYK for a symmetric polymer-polymer interface, and its relationship to the real-valued HT solution. Both solutions describe an interface in an incompressible blend of A and B polymers of equal degree of polymerization, N, and equal statistical segment length, a, with a Flory-Huggins interaction parameter χ , in the limit $\chi N \to \infty$. In the HT solution of this problem, the fields acting on the A- and B-type species, $w_A(z) = w_+(z) + w_-(z)$ and $w_B(z) = w_+(z) - w_-(z)$, respectively, are given in terms of

$$w_{-}(z) = \frac{\chi N}{2} \tanh\left(\frac{2(z-z_0)}{d_I}\right) \tag{2}$$

$$w_{+}(z) = \frac{3\chi N}{4} \tanh^{2}\left(\frac{2(z-z_{0})}{d_{I}}\right)$$
(3)

where z denotes a coordinate normal to the interface and $d_I = 2a/\sqrt{6\chi}$ is the width of the interface. An unspecified parameter z_0 is included in eqs 2 and 3 to account for the fact that the position of the interface is arbitrary. As a result of this translational invariance, the HT solution generates a 1D family of real-valued saddle-points parameterized by the real variable z_0 .

The family of complex-valued solutions derived by KYK for this interface problem actually has an identical form to that of eqs 2 and 3. The only differences are that the parameter z_0 is replaced by a purely-imaginary number, given in their notation by $z_0 = -i\theta d_I/2$, while the real function $\tanh(x)$ is replaced by its analytic continuation. This formal similarity suggests an interpretation whereby the 1D family of solutions is generated through translations of the real HT solution by imaginary displacements. Likewise, one could expect an even larger family of solutions generated by complex displacements, where z_0 assumes complex values.

Generalized Translational Invariance. In order to generalize this interpretation, we hereafter restrict our attention to models in which the Hamiltonian, H[w], is translationally invariant. This condition holds for all the situations considered by KYK, as their models did not include any external field that could explicitly distinguish different positions in space. Consequently, their models yield real SCFT solutions that can be translated by real displacements without affecting the value of the Hamiltonian. Furthermore, we assume that H[w] is an analytic functional of the fields, which is required for the validity of CL simulations.

It is straightforward to show that an invariance under generalized 'complex' translations is an automatic feature of any model with a H[w] that is both translationally invariant and analytic. For a polymeric system involving M monomer species in a D-dimensional space, H[w] is a complex-valued functional of complex-valued species fields, $w_i(\mathbf{r})$, for i=1, 2,...,M, which are all functions of a position vector, \mathbf{r} , with real Cartesian components, r_{μ} , for $\mu=1,2,...,D$. The assumption that H[w] is analytic implies the following: If infinitesimal perturbations of the fields, $\delta w_i(\mathbf{r})$, generate a perturbation of the Hamiltonian, δH , then field perturbations of $c\delta w_i(\mathbf{r})$ must generate a Hamiltonian perturbation of $c\delta H$, for any complex constant c. This statement is a straightforward generalization of how we define analyticity for a function of a single variable. To characterize translational invariance, it is convenient to consider an infinitesimal translation along some direction μ by a distance δv_{μ} . Such a translation yields a corresponding perturbation of the field by

$$\delta w_i(\mathbf{r}) = \delta v_\mu \frac{\partial w_i(\mathbf{r})}{\partial r_\mu} \tag{4}$$

which, in turn, causes a perturbation of the Hamiltonian by

$$\delta H[w] = \sum_{i=1}^{M} \int \delta w_i(\mathbf{r}) \frac{\delta H[w]}{\delta w_i(\mathbf{r})} d\mathbf{r}$$
 (5)

If H[w] is translationally invariant, then $\delta H[w] = 0$ for any perturbation of the above form. If H[w] is also analytic, then $\delta H[w] = 0$ for any infinitesimal complex displacement δv_{μ} , because

 δv_{μ} appears as a prefactor in the definition of $\delta w_{i}(\mathbf{r})$ given in eq 4. Thus, the combination of analyticity and invariance under translations by infinitesimal real displacements necessarily implies invariance under rigid translations by a broader class of 'complex' displacements. Moreover, invariance under infinitesimal complex displacements implies invariance under finite complex displacements, since these can be generated through the repeated application of infinitesimal complex displacements.

The analysis by KYK focused entirely on the nature of saddle-point configurations. The argument given above implies, however, that the invariance of H[w] is not a special property of saddle-points. For any field configuration with components $w_i(\mathbf{r})$, which need not be a saddle-point configuration, there exists an infinite set of field configurations with the same value of H[w], where each member of the set, $w_i(\mathbf{r}-\mathbf{v})$, is related to the original configuration by a complex displacement, \mathbf{v} .

Fourier-Space Representation. The effect of translation upon a field by a real displacement is easy to visualize. However, the numerical examples presented by KYK demonstrate that the effect by an imaginary displacement is more complicated and difficult to visualize. However, it does have a simple representation in Fourier space. Here and throughout, we focus our attention on fields that satisfy periodic boundary conditions, which is the typical case in SCFT calculations and CL-FTSs. For those systems defined in infinite domains, such as the HT interface problem, we can approximate the domain by a large finite volume with periodic boundaries and take the limit where one or more of the dimensions extends to infinity.

Now consider a complex-valued periodic function, $f(\mathbf{r})$, with a Fourier series representation

$$f(\mathbf{r}) = \frac{1}{V} \sum_{\mathbf{k}} \hat{f}(\mathbf{k}) e^{i\mathbf{k} \cdot \mathbf{r}}$$
 (6)

where the sum extends over all wavevectors \mathbf{k} that are compatible with the periodic boundary conditions (i.e., reciprocal lattice vectors). Using this Fourier representation, it is straight-

forward to show that a translation by the complex vector \mathbf{v} creates a displaced function

$$g(\mathbf{r}) = f(\mathbf{r} - \mathbf{v}) \tag{7}$$

with Fourier components of

$$\hat{g}(\mathbf{k}) = \hat{f}(\mathbf{k})e^{-i\mathbf{k}\cdot\mathbf{v}} \tag{8}$$

The effect of translation by a real displacement \mathbf{v} is to alter the phases of the Fourier coefficients, while maintaining their absolute magnitudes. Consider instead a displacement $\mathbf{v} = i\mathbf{u}$ with purely imaginary components, where \mathbf{u} is a real vector. The effect is to alter the absolute magnitudes by increasing $|\hat{g}(\mathbf{k})|$ for wavevectors where $\mathbf{k} \cdot \mathbf{u} > 0$ and by decreasing $|\hat{g}(\mathbf{k})|$ for wavevectors where $\mathbf{k} \cdot \mathbf{u} < 0$. Hence, an imaginary translation of a real-valued function $f(\mathbf{r})$ with $\hat{f}(-\mathbf{k}) = \hat{f}^*(\mathbf{k})$ produces a complex-valued function $g(\mathbf{r})$ with $\hat{g}(-\mathbf{k}) \neq \hat{g}^*(\mathbf{k})$.

Implications for CL-FTS. In complex-Langevin (CL) simulations, the fields take on arbitrary complex values at each point in space, and are sampled by a diffusion process defined by the CL equations.^{3–5} The form of the CL equations for AB-type systems is specified in the Supporting Information. CL sampling is expected to provide correct averages for observables, provided the CL diffusion process exhibits ergodic dynamics, i.e., if the probability distribution approaches a unique stationary distribution, P[w], in the limit of infinite time, $\tau \to \infty$.⁵ This P[w] is a real-valued probability-density functional in a complex function space, and is distinct from the complex Boltzmann weight, $P_c[w] = \exp(-H[w]/k_BT)$. Unlike for $P_c[w]$, there is no known explicit expression for P[w].

If the Hamiltonian, H[w], of a field-theoretic model is translationally invariant, then so are the associated CL equations, because the deterministic forces in the CL equations are functional derivatives of the Hamiltonian and the distribution of the random forces is independent of position. Furthermore, if a CL model has an analytic Hamiltonian that is invariant under generalized translations and the model exhibits ergodic dynamics, then the associated equilibrium distribution, P[w], must also be invariant under all generalized translations, as we will show below. Hence, in ergodic CL-FTSs of translationally-invariant models, field configurations that are related by a rigid complex translation are visited with equal frequency.

To prove the translational invariance of the equilibrium distribution, we consider the Fokker-Planck equation for the time-dependent probability distribution $P(\tau, [w])$ generated by a CL diffusion process. The Fokker-Planck equation takes the form $\partial P/\partial \tau = FP$, where F is a linear Fokker-Planck operator. Thus, stationary distributions are solutions of the homogeneous equation, FP = 0. Let $T_{\mathbf{v}}$ denote a translation operator that applies a rigid translation by a complex displacement \mathbf{v} to a probability distribution functional. For any translationally-invariant model with an analytic Hamiltonian, F and $T_{\mathbf{v}}$ must commute, such that $FT_{\mathbf{v}}P = T_{\mathbf{v}}FP$ for any complex \mathbf{v} and any distribution P. If P is stationary, it then follows that $P' \equiv T_{\mathbf{v}}P$ is also stationary, since $FT_{\mathbf{v}}P = T_{\mathbf{v}}FP = T_{\mathbf{v}}0 = 0$. Assuming there exists only one stationary distribution, P = P' implying that $P = T_{\mathbf{v}}P$ for any \mathbf{v} . Hence, the stationary distribution P[w] can only be unique if it is also translationally invariant.

Translationally-Invariant Analytic Observables. Results of CL-FTSs for observable physical quantities are typically obtained from ensemble averages of operators, O[w], defined as functionals of the fields. The theory underlying the CL method stipulates that valid averages, $\langle O[w] \rangle$, can only be obtained for analytic functionals. The existence of translational invariance further constrains the selection of quantities that can be unambiguously measured.

As a simple example, consider the process by which we identify the appearance of periodic order. We know that an infinitely-long CL-FTS in a finite volume would, in principle, give an uninformative homogeneous value for the average $\langle w_i(\mathbf{r}) \rangle$ of any field component. This is true even for an ordered phase, because the ordered phase can drift in a manner that would eventually wash out any inhomogeneities. The general lesson is that one should only measure translationally-invariant observables when simulating a translationally-invariant system.

The emergence of translational order associated with a unit cell smaller than the simu-

lation box can effectively be identified in a translationally-invariant manner by examining the behavior of the structure factor, particularly through the appearance of Bragg peaks. ¹⁸ In CL-FTSs, the structure factor, which is the Fourier transform of a density correlation function, is directly related to

$$G_{ij}(\mathbf{k}) = \frac{1}{V} \langle \hat{w}_i(\mathbf{k}) \hat{w}_j(-\mathbf{k}) \rangle \tag{9}$$

where $\hat{w}_i(\mathbf{k})$ is the Fourier amplitude of $w_i(\mathbf{r})$, as defined in eq 6. Using the Fourier representation of generalized translations provided in eq 8, it is straightforward to confirm that the value of $G_{ij}(\mathbf{k})$ remains invariant under arbitrary generalized translations. This ensures that field configurations related by generalized translations yield equal values for $G_{ij}(\mathbf{k})$ and any physical quantity (such as the structure factor) that can be expressed as a function of $G_{ij}(\mathbf{k})$.

The arguments presented above for the invariance of H[w] under generalized rigid translations rely solely on the existence of analyticity and translational invariance. Therefore, these arguments also extend to any observable that exhibits both of these properties. If O[w] is a translationally-invariant analytic functional of a field configuration w, then the value of O[w] will be identical for field configurations related by generalized rigid translations. The invariance of $G_{ij}(\mathbf{k})$ under generalized translations is a special case of this principle, as $G_{ij}(\mathbf{k})$ can be shown to be a translationally-invariant analytic functional of w. Generally, a functional of w that can be expressed as a polynomial in field components must be analytic. A product of Fourier components evaluated at wavevectors that add to zero is translationally invariant, whereas one where the sum of the wavevectors is not equal to zero is not. Consequently, $G_{ij}(\mathbf{k})$ is both analytic and translationally invariant. The Leibler free-energy functional derived for block copolymer melts is another example that satisfies these criteria for analyticity and translational invariance. However, functionals that involve complex conjugation or absolute magnitude operations are generally not analytic. For example,

 $|w_i(\mathbf{k})|^n$ with a non-negative integer n is not analytic, whereas $[w_i(\mathbf{k})w_j(-\mathbf{k})]^n$ is analytic. In CL-FTSs of translationally-invariant systems, it is therefore only safe to compute averages of translationally-invariant analytic functionals of the fields. Such 'allowed' observables are guaranteed to yield equal values for states related by generalized translations.

Self-Consistent Field Theory

In this section, SCFT is used to illustrate the effect of translation by imaginary displacements (i.e., $\mathbf{r} \to \mathbf{r} - i\mathbf{u}$) on the interface of an A/B homopolymer blend and the lamellar and cylindrical phases of an AB diblock copolymer melt. The SCFT calculations utilize the standard Gaussian chain model (GCM), treating the systems as incompressible melts of continuous elastic threads subject to Flory-Huggins interactions. The SCFT calculations are executed using the pseudospectral method, and imaginary translation of $\mathbf{v} = i\mathbf{u}$ is applied in Fourier space, the fields $\hat{w}_{\pm}(\mathbf{k})$ transform to $\hat{w}_{\pm}(\mathbf{k})e^{\mathbf{k}\cdot\mathbf{u}}$, simplifying the process to multiplication by appropriate exponential factors. Its implementation on equally-spaced Cartesian grids is straightforward, although complex-to-complex Fast Fourier Transforms (FFTs) are now employed for the complex SCFT calculation. As usual, the self-consistency conditions for the fields are solved iteratively, but here we continue the iterations until the relative change in the field drops below 10^{-9} to ensure precise saddle-point solutions.

Homopolymer Interface. We begin by examining the A/B interface of the symmetric homopolymer blend at $\chi N = 40$. The one-dimensional SCFT calculation is conducted in the canonical ensemble for a system of size $L_z = 5R_0$, where $R_0 = aN^{1/2}$, employing periodic boundary conditions. To obtain high accuracy, we use a fine spatial grid with $m_z = 2000$ points and discretize the polymer contour with steps of ds = 0.001. Once the real SCFT solution is obtained, we apply an imaginary translation, transforming the fields $w_{\pm}(z)$ to $w_{\pm}(z - iu_z)$. For $u_z < 0.0015R_0$, the field transformation yields a nearly perfect complex

saddle-point, where our self-consistency threshold is achieved after just one iteration. However, as the imaginary translation increases, it becomes necessary to apply more and more iterations until eventually they fail to converge. The failure is attributed to numerical errors introduced by exponentially growing multiplication factors. For instance, when a displacement of $\delta u_z = 0.01R_0$ is applied for $m_z = 2000$, the first harmonic for positive k_z grows by a factor of $e^{2\pi\delta u_z/L_z} \approx 1.0126$. However, the second harmonic increases by 1.0126^2 , and ultimately the 999th harmonic increases by 2.831×10^5 . Note that the final 1000th harmonic is held constant, given that it does not depend on the sign of k_z . We find that this minimizes the numerical inaccuracy arising from the finite grid spacing.

Considering the size of the multiplication factors, it is not surprising that the SCFT solution becomes inaccurate for large imaginary displacements. To stay within the family of complex saddle-points, we apply small successive translations of $\delta u_z = 0.01R_0$ and adjust the fields to satisfy the saddle-point conditions after each translation. Figure 1 shows the progression as the total distance from the real saddle-point, u_z , increases. Initially, convergence remains excellent, requiring only a few iterations to maintain self-consistency. However, as the total translation increases, more iterations are needed. The successive translation approach proves successful up to $u_z = 0.08R_0$, but beyond that the iteration fails to converge. Notably, this distance is approaching the point $u_z = \pi d_I/4$, where both the real and imaginary parts of the strong-segregation solution

$$w_{-}(z) \simeq \frac{\chi N}{2} \tanh\left(\frac{2(z - iu_z)}{d_I}\right)$$
 (10)

diverge at the interface. This rapid growth of the fields is readily apparent in Figure 1.

Diblock Copolymer Melt. We now turn our attention to the lamellar phase of an AB diblock copolymer melt at an A fraction of f = 0.5 and a segregation of $\chi N = 12$. In this case, the box size is set to the equilibrium lamellar period, $L_z = D_{eq} = 1.40R_0$, and the number of grid points is set to $m_z = 700$. For the real solution, the composition field

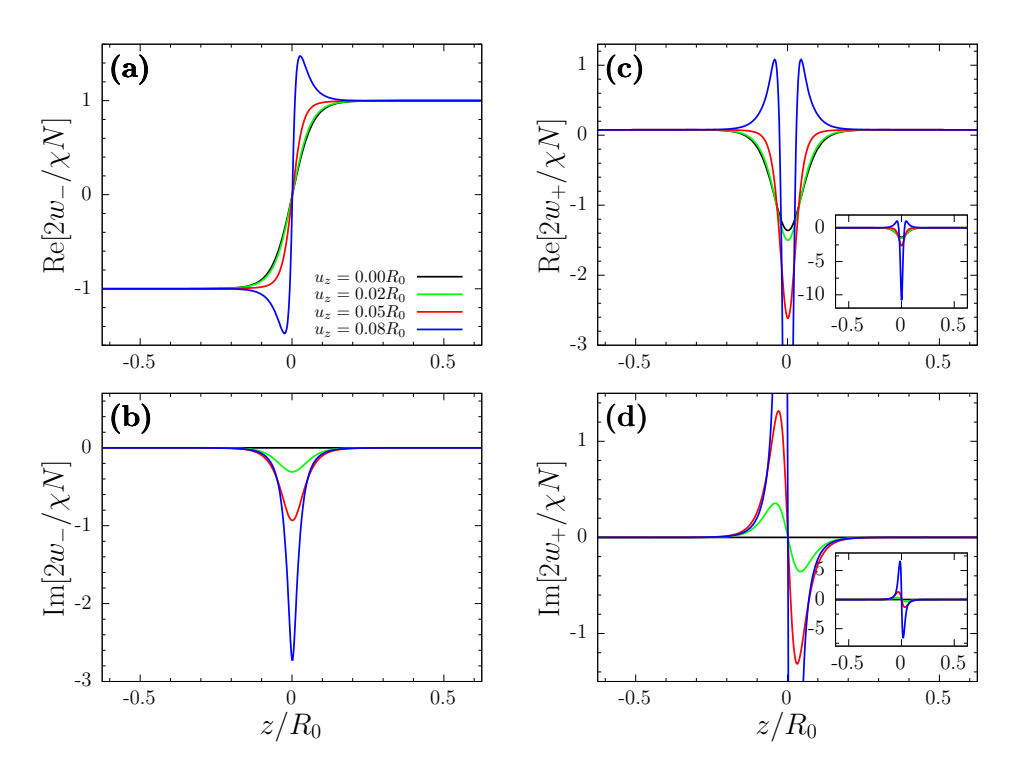


Figure 1: Complex saddle-point solution for an A/B homopolymer interface with $\chi N=40$, plotted for increasing imaginary distance, u_z , from the real saddle-point. The real and imaginary parts of $w_-(z)$ are shown in plots (a) and (b), respectively, and the real and imaginary parts of $w_+(z)$ are shown in plots (c) and (d), respectively. The insets show a reduced scale to capture the large field values for $u_z=0.08R_0$.

 $w_{-}(z)$ is dominated by the first harmonic, as depicted in Figure 2a. Conversely, the pressure field $w_{+}(z)$, shown in Figure 2c, is dominated by a much smaller second harmonic. This is a consequence of the A-B symmetry for f = 0.5. Figure 2 illustrates the result of successive imaginary translations by $\delta u_{z} = 0.01R_{0}$, starting from the real saddle-point. As required, the real value of the Hamiltonian is unaffected by the translations.

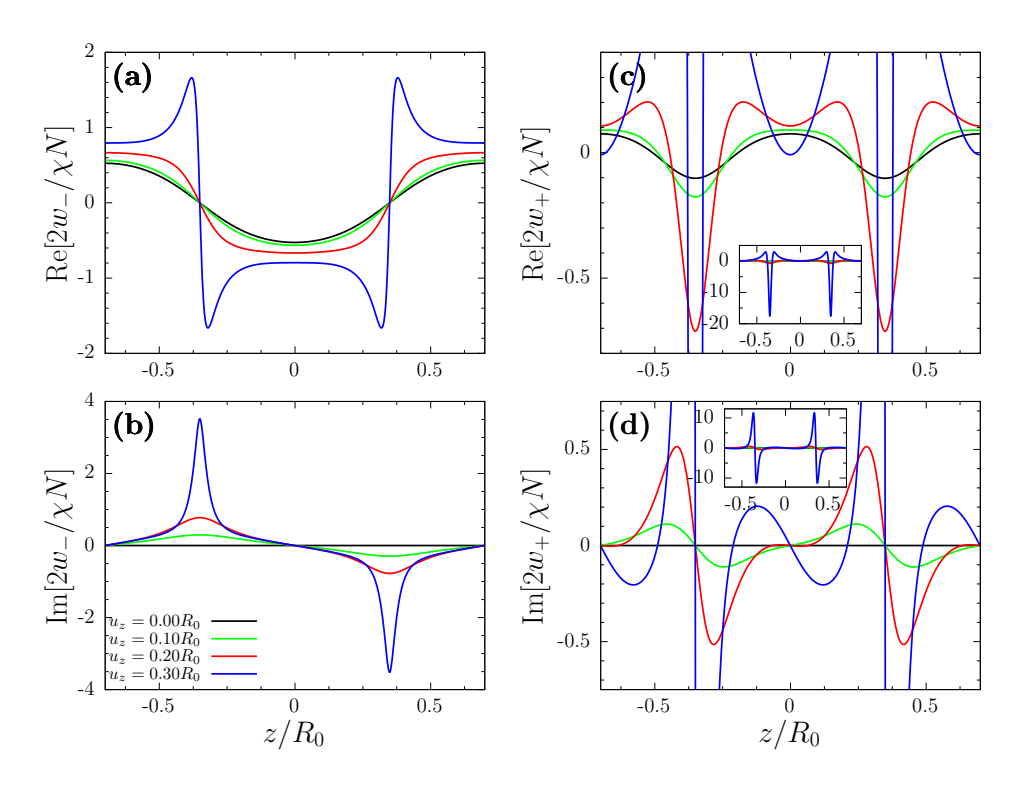


Figure 2: Complex saddle-point solution for an AB diblock copolymer lamellar phase with f = 0.5 and $\chi N = 12$, plotted for increasing imaginary distance, u_z , from the real saddle-point. The real and imaginary parts of $w_-(z)$ are shown in plots (a) and (b), respectively, and the real and imaginary parts of $w_+(z)$ are shown in plots (c) and (d), respectively. The insets show a reduced scale to capture the large field values for $u_z = 0.30R_0$.

As before, only a few iterations are required to maintain the self-consistent field equations in the vicinity of the real saddle-point. In this regime, the segregation is weak and therefore the composition field $w_{-}(z)$ is well approximated by

$$w_{-}(z) \simeq A\cos(k^{*}(z - z_{0} - iu_{z}))$$

$$= A\left[\cosh(k^{*}u_{z})\cos(k^{*}(z - z_{0})) + i\sinh(k^{*}u_{z})\sin(k^{*}(z - z_{0}))\right]$$
(11)

where $k^* \equiv 2\pi/D_{\rm eq}$. Note that we set the real part of the translation to $z_0 = 0$, such that ${\rm Re}[w_-(z)]$ and ${\rm Im}[w_-(z)]$ are even and odd functions of z, respectively. As u_z increases, the growth of higher harmonics causes the segregation to increase, which eventually invalidates the first-harmonic approximation in eq 11 and ultimately prevents the field iterations from converging for displacements beyond $u_z = 0.30R_0$. In the previous study, KYK presented saddle-points for a more segregated case, f = 0.5 and $\chi N = 25$. The results for this parameter set are shown in Figure S1 of the Supporting Information, but this time parameterized by the imaginary displacement, u_z . Due to the inherently larger harmonics, we were only able to translate the real saddle-point up to $u_z = 0.13R_0$.

The dimensionality of a family of complex saddle-points generally matches the dimensionality of the block copolymer morphology. To illustrate this, we consider the effect of imaginary displacements on a cylindrical morphology at f=0.4 and $\chi N=12$. For this calculation, we utilize spatial grids with $m_x=260$ and $m_y=150$, and we set ds=0.01. Images of its real saddle-point are displayed in Figure S2 of the Supporting Information. Given the 2D periodicity of the morphology, the translations now depend on direction as well as distance. To demonstrate the translation for a direction not aligned with any particular symmetry, we select $\delta \mathbf{u} = (0.006\hat{\mathbf{i}} + 0.008\hat{\mathbf{j}})R_0$ with a magnitude of $\delta u = 0.01R_0$. Again, we apply successive translations of $\delta \mathbf{u}$ and resolve the self-consistent conditions after each step. We achieved a maximum displacement of $|\mathbf{u}| = 0.32R_0$ before the fields fail to converge. The result for $|\mathbf{u}| = 0.05R_0$ is depicted in Figure 3. Additional examples for translations in the x- and y-directions are shown in Figures S2 and S3, respectively, of the Supporting Information. They experience similar translation limits of $|\mathbf{u}| = 0.31R_0$.

The real saddle-points considered here, as well as those examined by KYK, all possess inversion symmetry, $w_i(-\mathbf{r}) = w_i(\mathbf{r})$. Under imaginary translations, this symmetry generalizes to $w_i(-\mathbf{r}) = w_i^*(\mathbf{r})$. For this reason, KYK referred to their complex saddle-points as Hermitian. However, we now have a better understanding of the nature of this symmetry. The Hermitian property is not general and, in fact, it will not occur for morphologies without

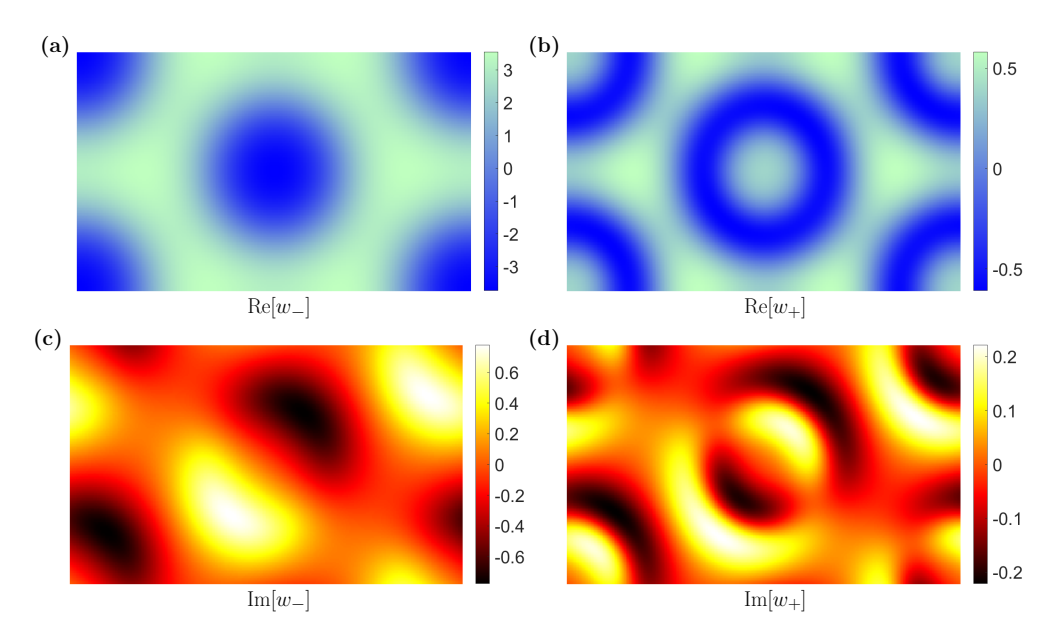


Figure 3: Complex SCFT solution for an AB diblock copolymer cylindrical phase with f = 0.4 and $\chi N = 12$, plotted for an imaginary displacement of $\mathbf{u} = (0.03\hat{\mathbf{i}} + 0.04\hat{\mathbf{j}})R_0$ from the real saddle-point. The real parts of $w_{-}(\mathbf{r})$ and $w_{+}(\mathbf{r})$ are shown in plots (a) and (b), respectively, and the imaginary parts are shown in plots (c) and (d), respectively. The size of each image is $2.70R_0 \times 1.56R_0$.

inversion symmetry, such as the single-gyroid phase. ^{21,22}

Complex-Langevin Field-Theoretic Simulations

We now illustrate the consequences of generalized translations on CL-FTSs of AB diblock copolymer melts, where the fields are permitted to explore the entire complex space. $^{4-6}$ The CL-FTSs are implemented as described in ref 23. In short, the diblock copolymers are modeled as discrete chains each with N=90 point-like beads connected by harmonic springs with a natural length of a_b . A fraction f of the beads are type A while the remaining beads are type B. The A and B beads are subject to pairwise contact interactions of the standard Flory-Huggins type, where χ_b controls the degree of immiscibility. The melt is compressible with a Helfand compressibility factor of $\zeta=1$, 17 which allows the local monomer density to vary slightly from $\rho_0=nN/V$, where n is the total number of molecules and V is the volume of the system. Note that ref 23 defined their fields as potential energies per monomer,

whereas here we define them as potential energies per chain.

Although the CL-FTSs are performed on a different model from that of the SCFT calculations, we define effective parameters, a and χ , using a Morse calibration. 24,25 This calibration maps the simulation results onto the standard GCM, which has the added benefit of removing an ultraviolet divergence that occurs in FTSs involving contact forces. Our current study is conducted at a high invariant polymerization index of $\bar{N} \equiv a^6 \rho_0^2 N = 10^6$, where the UV divergence is relatively weak. Therefore, we approximate the effective segment length as $a \approx a_b$ and the effective Flory-Huggins parameter by the linear approximation $\chi \approx z_{\infty} \chi_b$, where the expression for the proportionality factor, z_{∞} , can be found in ref 23.

Results. For simplicity, we limit our attention to the lamellar phase of symmetric AB diblock copolymers (f = 0.5), where the family of complex saddle-points is 1D. The CL-FTSs are performed on three lamellae oriented normal to the z direction in a cubic simulation box with periodic boundaries. The box size is set to $L_{\mu} = 4.2R_0$, and the fields are represented on a grid with $m_{\mu} = 32$ nodes in each dimension μ . For the resulting grid resolution, $z_{\infty} = 0.985$. We select the same value $\chi N = 12$ examined by SCFT in the preceding section. At this relatively weak segregation, the pressure field, $w_{+}(z)$, is approximately zero and the composition field can be approximated by the first harmonic

$$w_{-}(\mathbf{r}) \simeq A_R \cos(k^*(z - z_R)) + iA_I \cos(k^*(z - z_I))$$
(12)

where A_R , A_I , z_R , and z_I are real-valued. Although imaginary translations could potentially cause the higher harmonics to become significant, we find that the CL-FTSs always break down before this happens.

Figure 4 plots the amplitudes, A_R and A_I , in the upper graph and the relative phase angle of the real and imaginary parts, $\theta \equiv k^*(z_I - z_R)$, in the lower graph from a CL-FTS of duration $\tau N = 10^6$ initialized with an equilibrated configuration from an L-FTS²⁶ (i.e., $A_I = 0$ at $\tau = 0$). Without loss of generality, we choose $A_R > 0$ and $0 \le \theta < \pi$. Referring to

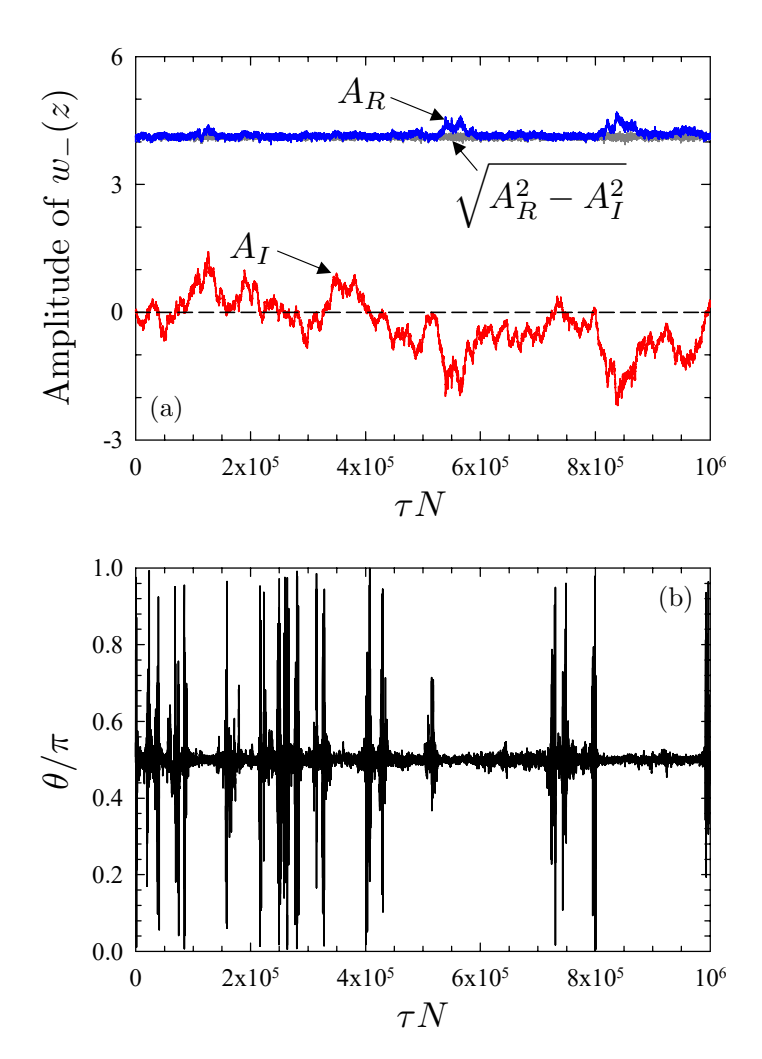


Figure 4: (a) Amplitudes of the first harmonics of $w_{-}(\mathbf{r})$ and (b) phase angle between the harmonics plotted as a function of simulation time, τ , during a CL-FTS of a lamellar phase for $\chi N = 12$ and $\bar{N} = 10^6$.

eq 11, we should expect the real and imaginary amplitudes to satisfy $A_R^2 - A_I^2 \approx A^2$, which is confirmed by the gray curve in Figure 4a. Likewise, $\theta \approx \pi/2$ whenever A_I develops an appreciable magnitude as illustrated in Figure 4b. Thus, the CL-FTS is clearly fluctuating about the line of complex saddle-points illustrated in Figure 2.

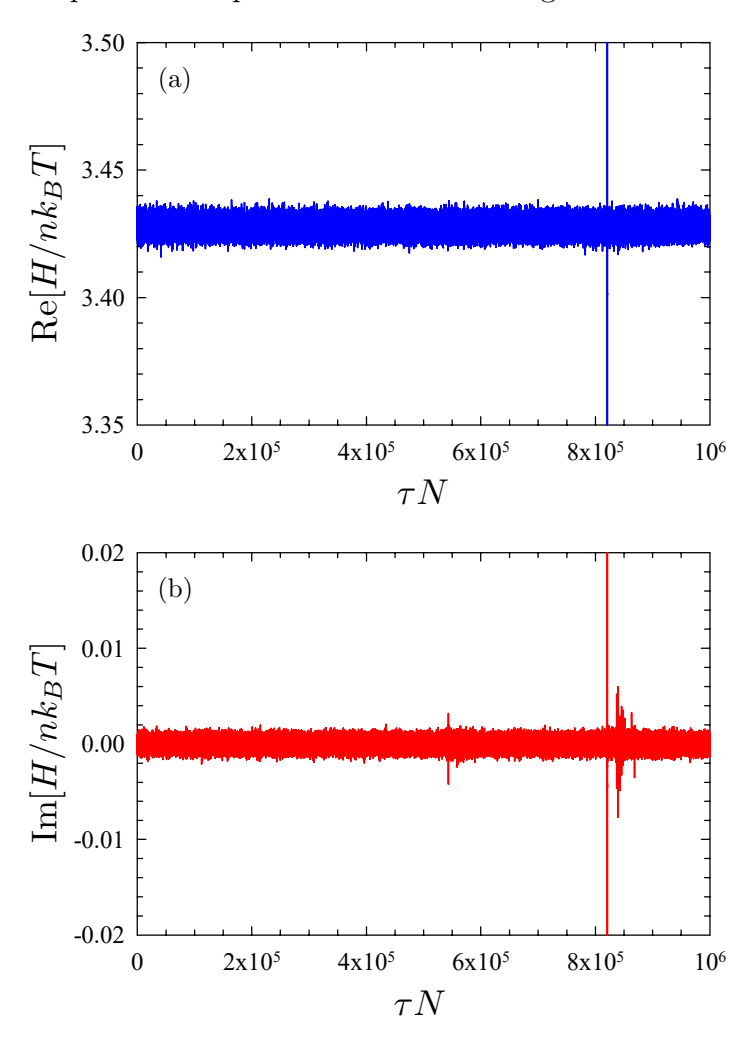


Figure 5: (a) Real and (b) imaginary parts of the Hamiltonian, H, sampled during the same CL-FTS from Figure 4. The large fluctuations for $\tau N \gtrsim 8.2 \times 10^5$ are due to the formation of a hot spot.

As evident from Figure 4, the system moves slowly along the line of complex saddlepoints, so much so that there is no hope of thoroughly sampling the full space. Fortunately though, the probability distribution for the complexified fields, P[w], and the observables of interest are translationally invariant, allowing for accurate averages without doing so. Figure 5 plots the real and imaginary parts of the Hamiltonian, H, as a function of simulation time, τ . Notably, the distribution of H appears uncorrelated with the position along the saddle-point line (we will confirm this later), at least for the initial part of the CL-FTS. At $\tau N = 8.2 \times 10^5$, however, a localized 'hot spot' emerges where the fields attain extreme values, primarily affecting the imaginary part of H but also influencing the real part to some extent. The occurrence of hot spots has been documented previously in refs 14 and 23. They are found to create tails in the distributions of observables, causing moments of the distributions to diverge.²³ This behavior is not new to CL simulations and is regarded as a failure of the method.^{27–30} Nevertheless, the distributions remain well-behaved prior to the hot spot. In this case, Figure 6 confirms that the real and imaginary parts of H before $\tau N = 8.2 \times 10^5$ are accurately described by Gaussian distributions. The real part has a mean of $\text{Re}[\langle H \rangle / nk_B T] = 3.4279$ and a standard deviation of $\sigma_R/nk_B T = 0.00248$, while the imaginary part is consistent with a mean of zero and a standard deviation of $\sigma_I/nk_B T = 0.00047$. Note that the imaginary part of any observable must average to zero, and indeed it always does when the CL-FTS is behaving properly.

Translation Cooling. Hot spots generally form when the system deviates significantly from the real saddle-point. ²³ Indeed, the hot spot at $\tau N = 8.2 \times 10^5$ emerged when $|A_I|$ reached its most extreme value. There is also a small spike in Im[H] suggesting a hot spot nearly formed at $\tau N = 5.4 \times 10^5$, where $|A_I|$ acquired a similarly large value. The failure of CL simulations in quantum chromodynamics (QCD) occurs in much the same way due to a gauge invariance. ^{30–33} In QCD, this is remedied by the continuous application of gauge transformations during the simulation, a method referred to as 'gauge cooling'. ^{34,35} Inspired by this, we devise an analogous method, which we refer to as 'translation cooling', where small imaginary translations of $\delta \mathbf{u}$ are repeatedly applied to $w_{-}(\mathbf{r})$ and $w_{+}(\mathbf{r})$ so as to shift the system towards the real saddle-point. As illustrated previously, the equilibrium probability distribution, P[w], should be invariant under complex translations, and therefore we expect the ensemble average of any translationally-invariant observable to be unaffected by the imaginary translations, just as it would be by real translations.

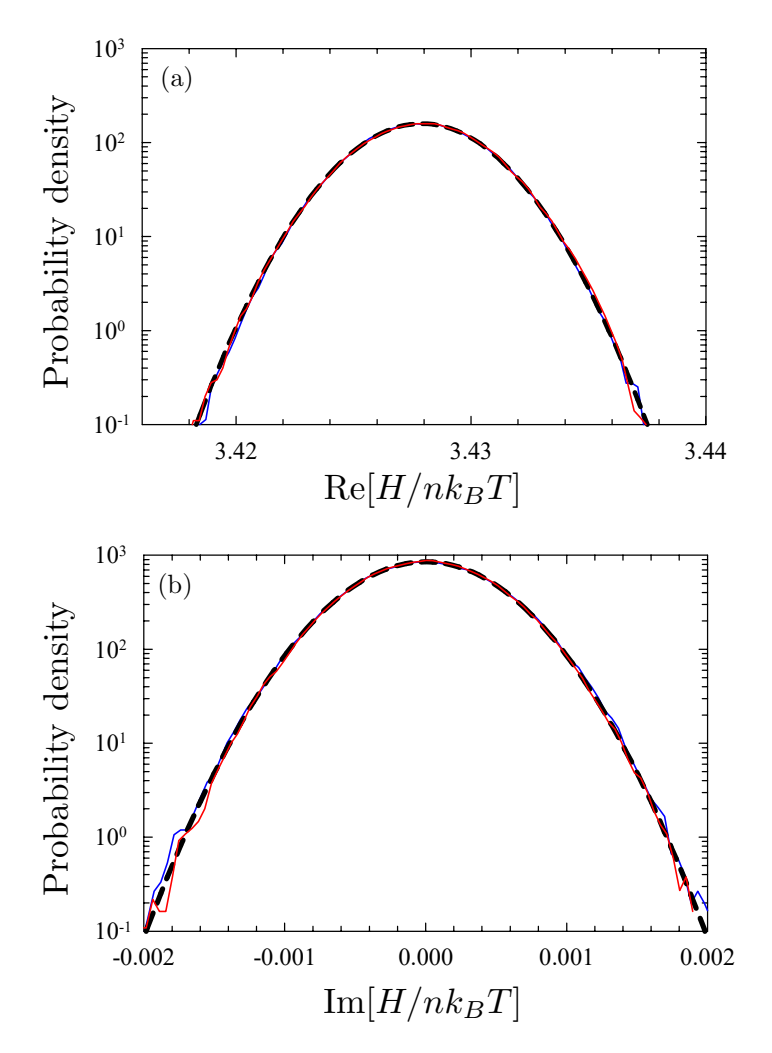


Figure 6: Histograms of the (a) real and (b) imaginary parts of the Hamiltonian, H, in CL-FTSs with (blue curves) and without (red curves) translation cooling, plotted on a logarithmic scale. The dashed curves are fits to Gaussian distributions.

Given that the imaginary part of $w_{-}(\mathbf{r})$ is zero at the real saddle-point, we design the translation cooling to minimize

$$\Gamma(\delta \mathbf{u}) \equiv \int |w_{-}(\mathbf{r} - i\delta \mathbf{u}) - w_{-}^{*}(\mathbf{r} - i\delta \mathbf{u})|^{2} d\mathbf{r}$$
(13)

$$= \frac{1}{(2\pi)^3} \int |e^{\mathbf{k}\cdot\delta\mathbf{u}} \hat{w}_{-}(\mathbf{k}) - e^{-\mathbf{k}\cdot\delta\mathbf{u}} \hat{w}_{-}^*(-\mathbf{k})|^2 d\mathbf{k}$$
 (14)

$$= \frac{2}{(2\pi)^3} \int |e^{2\mathbf{k}\cdot\delta\mathbf{u}} \hat{w}_{-}(\mathbf{k})|^2 d\mathbf{k} + \text{constant}$$
 (15)

where eq 15 is arrived at using Parseval's theorem and the relation in eq 8. It follows that the gradient of $\Gamma(\delta \mathbf{u})$ is

$$\frac{\partial \Gamma}{\partial \delta u_{\mu}} = \frac{1}{2\pi^3} \int k_{\mu} e^{2\mathbf{k} \cdot \delta \mathbf{u}} |\hat{w}_{-}(\mathbf{k})|^2 d\mathbf{k}$$
(16)

$$\approx B_{\mu} + \sum_{\nu=x,y,z} J_{\mu\nu} \delta u_{\nu} \tag{17}$$

where

$$B_{\mu} = \frac{1}{2\pi^3} \int k_{\mu} |\hat{w}_{-}(\mathbf{k})|^2 d\mathbf{k}$$

$$\tag{18}$$

$$J_{\mu\nu} = \frac{1}{\pi^3} \int k_{\mu} k_{\nu} |\hat{w}_{-}(\mathbf{k})|^2 d\mathbf{k}$$
 (19)

Provided that the system remains in close proximity to the real saddle-point, the imaginary translation required to minimize $\Gamma(\delta \mathbf{u})$ should be well approximated by

$$\delta \mathbf{u} = -\mathbf{J}^{-1}\mathbf{B} \tag{20}$$

Note that for the special case of a 1D lamellar phase, it is sufficient to apply the component δu_z normal to the lamellae. However, for the sake of algorithmic generality, we apply the full vector $\delta \mathbf{u}$.

The performance of this method is relatively insensitive to the frequency at which the

translations are applied. Therefore, to reduce the computational cost, they are not applied at every Langevin step, but nevertheless they are applied frequently. That way the system never drifts far from the real saddle-point and the magnitude of $\delta \mathbf{u}$ remains small as assumed by the linearization in eq 17. Having said that, there is no need for the gradient of $\Gamma(\delta \mathbf{u})$ to be accurately zero. All we require is that $\delta \mathbf{u}$ generally moves the system closer to rather than further from the real saddle-point.

Figure 7 presents results from a CL-FTS similar to that of Figure 4, but with imaginary translations applied at intervals of $\Delta \tau N = 5$. With translation cooling, the imaginary component of the field, A_I , now remains close to zero, implying that the system is fluctuating about the real saddle-point. The distribution of H with translation cooling (red curve) plotted in Figure 6 is indistinguishable from the previous distribution without cooling (blue curve), to within the level of the statistical uncertainty. The difference now is that we can run the CL-FTS indefinitely without the formation of hot spots.

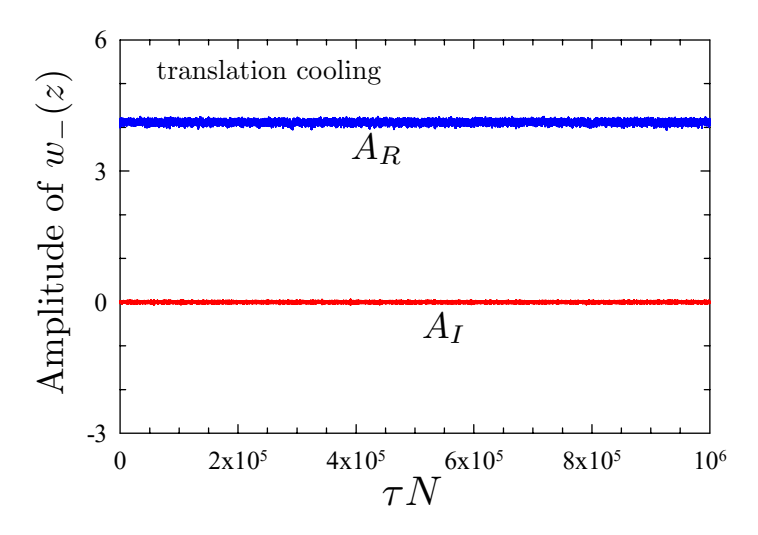


Figure 7: Analogous plot to Figure 4a, but with translation cooling.

We can, likewise, investigate different positions along the family of complex saddle-points, corresponding to nonzero gradients of $C_{\nu} = \partial \Gamma / \partial \delta u_{\nu}$, by performing translations of

$$\delta \mathbf{u} = \mathbf{J}^{-1}(\mathbf{C} - \mathbf{B}) \tag{21}$$

The amplitude of the fluctuations is similar, but the averages of A_I are now shifted (see Supporting Information) as are the averages of A_R . Table 1 lists the averages for several different values of C_z . The fact that $\langle A_R \rangle^2 - \langle A_I \rangle^2$ remains approximately constant confirms that the system is fluctuating about a complex saddle-point. The total distance of the complex saddle-point from the real one can be estimated by

$$u_z = \frac{1}{k^*} \tanh^{-1} \left(\frac{\langle A_I \rangle}{\langle A_R \rangle} \right) \tag{22}$$

However, there is a limited range of over which the simulations remain stable. If we set $C_z \gtrsim 1.8$, the system starts to form hot spots.

In the absence of hot spots, the CL-FTS behaves well as evident by the fact that the distribution of H remains Gaussian. Table 2 lists the mean and standard deviations of H at different points along the line of saddle-points. Interestingly, $\langle H \rangle$ maintains a constant real value across the entire line. Even the width of the Gaussians is constant for the real part of H and nearly constant for the imaginary part. Admittedly, there is a small but noticeable increase in σ_I as the imaginary distance from the real saddle-point, u_z , increases (see Supporting Information). We attribute this to hot-spot-like fluctuations, which presumably become more frequent as the system moves away from the real saddle-point. Recall that the hot spots have a more pronounced effect on the imaginary part of H than the real part.

Table 1: Average Amplitudes of the Real and Imaginary Parts of the Composition Field and Imaginary Distance to the Real Saddle-Point.

C_z	$\langle A_R \rangle$	$\langle A_I \rangle$	$\sqrt{\left\langle A_R ight angle^2 - \left\langle A_I ight angle^2}$	$\frac{u_z}{R_0}$
0.0	4.115	0.000	4.115	0.000
0.3	4.126	0.312	4.114	0.017
0.6	4.161	0.617	4.115	0.033
0.9	4.213	0.907	4.114	0.049
1.2	4.281	1.185	4.113	0.063
1.5	4.361	1.443	4.115	0.077

The distribution of the imaginary translations normal to the lamellae, δu_z , required to

Table 2: Mean and Standard Deviations of the Real and Imaginary Parts of the Hamiltonian at Different Positions Along the Line of Complex Saddle-Points.

C_z	$\frac{\operatorname{Re}[\langle H \rangle]}{nk_BT}$	$rac{\sigma_R}{nk_BT}$	$\frac{\mathrm{Im}[\langle H \rangle]}{nk_BT}$	$rac{\sigma_I}{nk_BT}$
0.0	3.4279	0.00249	0.0000	0.00046
0.3	3.4280	0.00250	0.0000	0.00046
0.6	3.4279	0.00248	0.0000	0.00047
0.9	3.4280	0.00248	0.0000	0.00049
1.2	3.4279	0.00249	0.0000	0.00050
1.5	3.4280	0.00418	0.0000	0.00092

maintain fixed positions along the line of complex saddle-points is plotted in Figure 8. In all cases, the distribution is centered about $\delta u_z = 0$, indicating there is no effective force driving the system in either direction along the line. Consequently, without the translation cooling, the system would simply diffuse along the line of complex saddle-points. Interestingly, the width of the distribution, and thus the diffusion constant, increases as the system moves farther from real saddle-point. In any case, the fact that the motion is naturally diffusive means that if the translation cooling were to be turned off then the system would eventually reach a point where hot spots form.

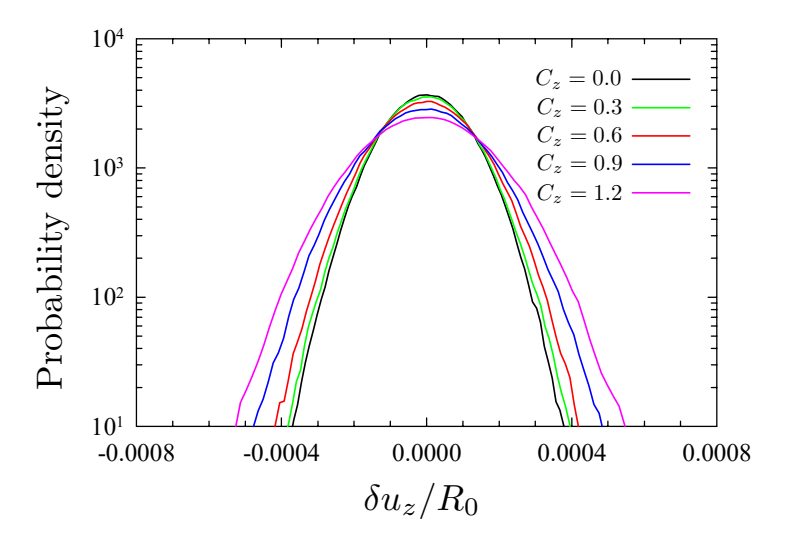


Figure 8: Distribution of the imaginary translations perpendicular to the lamellae, δu_z , required to maintain different positions along the line of complex saddle-points.

In our study with $\chi N=12$ and $\bar{N}=10^6$, CL-FTSs remain stable with respect to the formation of hot spots as long as $|u_z|\lesssim 0.07R_0$. Unfortunately, this stability region mono-

tonically shrinks and eventually vanishes as χN approaches the order-disorder transition, and hot spots form even with translation cooling. The problem is further exacerbated as \bar{N} is reduced. We thus envision translation cooling as being used in conjunction with other methods of improving stability. We note that Delaney and Fredrickson⁶ were able to run stable CL-FTSs down to $\bar{N} \approx 10^4$ with the use of nonzero-range interactions, although the range was unrealistically large. It is conceivable that a more reasonable range would suffice if a nonzero-range interaction was supplemented with translation cooling.

Summary

In SCFT, the phases of a polymeric system are associated with real-valued saddle-points of its field-theoretic Hamiltonian, H[w]. Kang, Yong, and Kim¹⁵ have recently found a number of examples where the real-valued saddle-points are connected to continuous families of complex-valued saddle-points that share the same real value of H[w]. Here, we showed that this behavior is general to all systems with translational symmetry, such as the bulk phases of a block copolymer melt. Assuming that H[w] is an analytic functional of the fields, $w_i(\mathbf{r})$, it immediately follows that any system that is invariant under normal translations (i.e., $\mathbf{r} \to \mathbf{r} - \mathbf{v}$ for real \mathbf{v}) must also be invariant under translation by a complex displacement. As such, a family of complex-valued saddle-points can be generated by applying imaginary translations (i.e., $\mathbf{v} = i\mathbf{u}$) to the real saddle-point. As usual, translations have no effect in directions where $w_i(\mathbf{r})$ remains constant, and thus the dimensionality of the continuous family is equal to the number of independent directions in which $w_i(\mathbf{r})$ varies. Here, we have demonstrated this for the 1D homopolymer-homopolymer interface, the 1D diblock copolymer lamellar phase, and the 2D diblock copolymer cylindrical phase.

Although the complex saddle-points are unphysical SCFT solutions, they nevertheless have profound implications for CL-FTSs. Rather than fluctuating about isolated real saddle-points, the fields in a CL-FTS fluctuate about a continuous family of complex saddle-points

emanating from a real saddle-point. Here, we demonstrated this for the 1D diblock copolymer lamellar phase. We find that there is no effective force and therefore the system generally diffuses along the line of saddle-points, although with a diffusion constant that increases with $|\mathbf{u}|$, the imaginary distance from the real saddle-point.

Our SCFT calculations demonstrate that the fields develop extreme values as $|\mathbf{u}|$ becomes large relative to the width of the A/B interfaces. Consequently, the CL-FTSs will fail without anything to prevent diffusion to large $|\mathbf{u}|$. The failure generally occurs via the spontaneous formation of delta-like 'hot spots', as observed previously. 14,23 However, in many cases, we are able to remedy the problem with translation cooling, where small imaginary translations, $\delta \mathbf{u}$, are continuously applied so as to maintain close proximity to the real saddle-point. Unfortunately, the propensity to form hot spots becomes so great near the order-disorder transition and at low \bar{N} that the CL-FTSs often fail even with the use of translation cooling. Nevertheless, there is good reason to hope that translation cooling could be combined with appropriate modifications to the polymeric model, such as nonzero-range interactions, to produce robust CL-FTSs.

Supporting Information

Field-theoretic model for a diblock copolymer melt, discussion regarding the analyticity of polymer field theory, additional SCFT examples for the lamellar and cylindrical phases of diblock copolymer melts, and CL-FTS results for translation cooling with $C_z \neq 0$.

Acknowledgments

JUK acknowledges the National Research Foundation of Korea (NRF) grant funded by the Korea government (MSIT) Grant Nos. RS-2023-00257666 and RS-2024-00348534. MWM acknowledges the Natural Sciences and Engineering Research Council (NSERC) of Canada and the Digital Research Alliance of Canada. DCM acknowledges the National Science Foundation.

tion (NSF) Grant No. OAC-2103627.

References

- (1) Matsen, M. W. The standard Gaussian model for block copolymer melts. *J. Phys.:* Condens. Matter **2002**, 14, R21–R47.
- (2) Fredrickson, G. H. *The Equilibrium Theory of Inhomogeneous Polymers*; Oxford University Press: Oxford, 2006.
- (3) Matsen, M. W. Field theoretic approach for block polymer melts: SCFT and FTS. *J. Chem. Phys.* **2020**, *152*, 110901.
- (4) Fredrickson, G. H.; Ganesan, V.; Drolet, F. Field-Theoretic Computer Simulation Methods for Polymers and Complex Fluids. *Macromolecules* **2002**, *35*, 16–39.
- (5) Fredrickson, G. H.; Delaney, K. T. Field-Theoretic Simulations in Soft Matter and Quantum Fluids; Oxford University Press: Oxford, 2023.
- (6) Delaney, K. T.; Fredrickson, G. H. Recent Developments in Fully Fluctuating Field-Theoretic Simulations of Polymer Melts and Solutions. J. Phys. Chem. B 2016, 120, 7615–7634.
- (7) Liu, Y.-X.; Delaney, K. T.; Fredrickson G. H. Field-Theoretic Simulations of Fluctuation-Stabilized Aperiodic "Bricks-and-Morta" Mesophase in Miktoarm Star Block Copolymer/ Homopolymer Blends. *Macromolecules* 2017, 50, 6263–6272.
- (8) Spencer, R. K. W.; Matsen, M. W. Field-theoretic simulations of bottlebrush copolymers. J. Chem. Phys. 2018, 149, 184901.
- (9) Spencer, R. K. W.; Matsen, M. W. Coexistence of polymeric microemulsion with homopolymer-rich phases. *Macromolecules* **2021**, *54*, 1329–1337.

- (10) Matsen, M. W.; Beardsley, T. M.; Willis, J. D. Fluctuation-corrected phase diagrams for diblock copolymer melts. *Phys. Rev. Lett.* **2023** *130*, 248101.
- (11) Willis J. D.; Matsen, M. W. Bicontinuous microemulsion in binary blends of complementary diblock copolymers. *J. Chem. Phys.* **2024**, *160*, 024906.
- (12) Ganesan, V.; Fredrickson, G. H. Field-Theoretic Polymer Simulations. Europhys. Lett. **2001**, *55*, 814–820.
- (13) Düchs, D.; Delaney, K. T.; Fredrickson, G. H. A multi-species exchange model for fully fluctuating polymer field theory simulations. *J. Chem. Phys.* **2014**, *141*, 174103.
- (14) Vigil, D. L.; Delaney, K. T.; Fredrickson, G. H. Quantitative Comparison of Field-Update Algorithms for Polymer SCFT and FTS. *Macromolecules* **2021**, *54*, 9804–9814.
- (15) Kang, W.; Yong, D.; Kim, J. U. Characteristics of the Complex Saddle Point of Polymer Field Theory. *Macromolecules* **2024**, *57*, 3850–3861.
- (16) Helfand, E.; Tagami, Y. Theory of the Interface Between Immiscible Polymers. *Polym. Lett.* **1971**, *9*, 741–746.
- (17) Helfand, E.; Tagami, Y. Theory of the Interface Between Immiscible Polymers. II *J. Chem. Phys.* **1972**, *56*, 3592–3601.
- (18) Beardsley, T. M.; Matsen, M. W. Fluctuation correction for the order–disorder transition of diblock copolymer melts. *J. Chem. Phys.* **2021**, *154*, 124902.
- (19) Leibler, L. Theory of Microphase Separation in Block Copolymers. *Macromolecules* **1980**, *13*, 1602–1617.
- (20) Rasmussen, K. O.; Kalosakas, G. Improved numerical algorithm for exploring block copolymer mesophases. *J. Polym. Sci.* **2002**, *40*, 1777–1783.

- (21) Xie, Q.; Li, W. Single Gyroid Self-Assembled by Linear BABAB Pentablock Copolymer *ACS Macro Lett.* **2022**, *11*, 205–209.
- (22) Park, S. J.; Bates, F. S.; Dorfman, K. D. Single gyroid in H-shaped block copolymers *Phys. Rev. Mater.* **2023**, *7*, 105601.
- (23) Matsen, M. W.; Willis, J. D.; Beardsley, T. M. Accurate Universal Predictions for Block Copolymer Melts Using Field-Theoretic Simulations. *Macromolecules* 2024, 57, 4312–4322.
- (24) Glaser, J.; Qin, J.; Medapuram, P.; Morse, D. C. Collective and Single-Chain Correlations in Disordered Melts of Symmetric Diblock Copolymers: Quantitative Comparison of Simulations and Theory. *Macromolecules* 2014, 47, 851–869.
- (25) Glaser, J.; Medapuram, P.; Beardsley, T. M.; Matsen, M. W.; Morse, D. C. Universality of Block Copolymer Melts. *Phys. Rev. Lett.* **2014**, *113*, 068302.
- (26) Matsen M. W.; Beardsley, T. M. Field-theoretic simulations for block copolymer melts using the partial saddle-point approximation. *Polymers* **2021**, *13*, 2437.
- (27) Nagata, K.; Nishimura, J.; Shimasaki, S. Argument for justification of the complex Langevin method and the condition for correct convergence. Phys. Rev. D 2016, 94, 114515.
- (28) Rammelmüller, L.; Porter, W. J.; Drut, J. E.; Braun, J. Surmounting the sign problem in nonrelativistic calculations: A case study with mass-imbalanced fermions. *Phys. Rev.* D 2017, 96, 094506.
- (29) Attanasio, F.; Jäger, B. Improved convergence of Complex Langevin simulations. *EPJ Web Conf.* **2018**, *175*, 07039.
- (30) Berger, C. E.; Rammelmüller, L.; Loheac, A. C.; Ehmann, F.; Braun, J.; Drut, J. E.

- Complex Langevin and other approaches to the sign problem in quantum many-body physics. *Phys. Reports* **2021**, *892*, 1–54.
- (31) Seiler, E. Status of Complex Langevin. EPJ Web Conf. 2018, 175, 01019.
- (32) Attanasio, F.; Jäger, B.; Ziegler, F. P. G. Complex Langevin simulations and the QCD phase diagram: recent developments. *Eur. Phys. J. A.* **2020**, *56*, 251.
- (33) Cai, Z.; Dong, X.; Kuang, Y. On the Validity of Complex Langevin Method for Path Integral Computations. SIAM J. Sci. Comput. 2021, 43, A685–A719.
- (34) Seiler, E.; Sexty, D.; Stamatescu, I. O. Gauge cooling in complex Langevin for QCD with heavy quarks. *Phys. Lett. B* **2013**, *723*, 213–216.
- (35) Aarts, G.; Bongiovanni, L.; Seiler, E.; Sexty, D.; Stamatescu, I. O. Controlling complex Langevin dynamics at finite density. *Eur. Phys. J. A* **2013**, *49*, 89.

Supporting Information: Complex Implications of Translational Invariance in Polymer Field Theory

Jaeup U. Kim, Mark W. Matsen,* David C. Morse,* and James D. Willis

E-mail: mwmatsen@uwaterloo.ca; morse012@umn.edu

Model and Notation

To clarify our notation and conventions, we discuss the construction of a field-theoretic Hamiltonian for a system of polymers involving two monomer types, denoted by A and B. This generally starts from a particle-based model with a potential energy of the form

$$U = U_{\text{bond}} + U_{\text{int}} \tag{S1}$$

where U_{bond} and U_{int} represent the bonded and non-bonded interactions, respectively. For a compressible system with contact forces, one usually chooses^{1,2}

$$U_{\text{int}} = k_B T v \int \left[\chi \rho_A(\mathbf{r}) \rho_B(\mathbf{r}) + \frac{1}{2} \zeta \left[\rho_A(\mathbf{r}) + \rho_B(\mathbf{r}) - \rho_0 \right]^2 \right] d\mathbf{r}$$
 (S2)

where $\rho_i(\mathbf{r})$ denotes the concentration of *i*-type monomers at position \mathbf{r} , v is an energetically-preferred monomer volume, $\rho_0 = 1/v$, χ is the Flory-Huggins interaction parameter, and ζ is a dimensionless compression modulus. The numerical examples in the associated paper considered binary homopolymer blends and diblock copolymer melts. For concreteness, we focus here on melts of n AB diblock copolymers in a region of volume V, where each diblock contains N monomers of which a fraction f forms the A block.

Field-Theoretic Hamiltonian. Use of Hubbard-Stratonovich transformations to define a field-theoretic representation of the partition function, Z, and adoption of complex-Langevin sampling yields a polymer field theory in which physical quantities are related to averages over configurations of two fields, $w_A(\mathbf{r})$ and $w_B(\mathbf{r})$. Details can be found in ref 2. Here, we defined our fields as dimensionless potential energies per chain, such that the monomers of type i in a chain of polymerization N each contribute a potential energy of $w_i(\mathbf{r})/N$. Note that this is slightly different from ref 2, where their fields, $W_i(\mathbf{r}) = w_i(\mathbf{r})/N$, were defined as potential energies per monomer.

The field-theoretic representation of Z involves a generalized Boltzmann weight $^{3-5}$

$$P_{c}[w] = e^{-H[w]/k_BT} \tag{S3}$$

defined by a field-theoretic Hamiltonian of the form

$$H[w] = -k_B T \ln Z_{id}[w] + H_f[w]$$
(S4)

The $H_f[w]$ contribution is generally a quadratic functional of the fields. For the compressible model with local interactions in eq S2,

$$H_{\rm f}[w] = \frac{k_B T}{v_{\rm p}} \int \left[\frac{w_-^2(\mathbf{r})}{\chi N} - \frac{w_+^2(\mathbf{r})}{(\chi + 2\zeta)N} - w_+(\mathbf{r}) + \frac{\chi N}{4} \right] d\mathbf{r}$$
 (S5)

where $v_{\rm p} \equiv Nv$ is a volume per polymer chain and

$$w_{\pm}(\mathbf{r}) = [w_A(\mathbf{r}) \pm w_B(\mathbf{r})]/2 \tag{S6}$$

The $Z_{id}[w]$ in eq S4 is the partition function of a hypothetical ideal gas with a potential energy

$$U_{\rm id} = U_{\rm bond} + \frac{k_B T}{N} \sum_{i=A|B|} \int \rho_i(\mathbf{r}) w_i(\mathbf{r}) d\mathbf{r}$$
 (S7)

evaluated in the same statistical ensemble used to describe the interacting system. In the canonical ensemble, it takes the form

$$Z_{\rm id}[w] = \frac{1}{n!} (VQ[w]/v_{\rm p})^n \qquad \text{(Canonical)}$$
(S8)

and in the grand-canonical ensemble, it is given by

$$Z_{id}[w] = \sum_{n=0}^{\infty} \frac{1}{n!} e^{\mu n/k_B T} (VQ[w]/v_p)^n$$

$$= \exp\left(e^{\mu/k_B T} VQ[w]/v_p\right) \qquad \text{(Grand canonical)} \tag{S9}$$

where μ is the polymer chemical potential. The functional Q[w] represents the partition function for a single polymer chain in which the A and B monomers are acted upon by the $w_A(\mathbf{r})$ and $w_B(\mathbf{r})$ fields, respectively. Explicit expressions for Q[w] will be provided later.

Complex-Langevin (CL) Sampling. In CL sampling, the $w_{-}(\mathbf{r})$ and $w_{+}(\mathbf{r})$ fields are allowed to explore arbitrary complex values, and they evolve under the CL equations. The discrete version of the CL equations for fields defined on a regular grid is given by

$$w_{-}^{(k+1)}(\mathbf{r}) = w_{-}^{(k)}(\mathbf{r}) - \Lambda_{-}^{(k)}(\mathbf{r}) \,\delta\tau N + \mathcal{N}(0,\sigma)$$
 (S10)

$$w_{+}^{(k+1)}(\mathbf{r}) = w_{+}^{(k)}(\mathbf{r}) + \Lambda_{+}^{(k)}(\mathbf{r}) \,\delta\tau N + i\mathcal{N}(0,\sigma)$$
 (S11)

where $w_{\pm}^{(k)}(\mathbf{r})$ are the field values at the k'th time step for grid position \mathbf{r} , $\delta \tau = \tau^{(k+1)} - \tau^{(k)}$ is the size of the k'th time step, $\Lambda_{\pm}^{(k)}(\mathbf{r})$ are deterministic forcing terms evaluated at the k'th time step, and $\mathcal{N}(0,\sigma)$ denotes a real-valued random number from a Gaussian distribution with zero mean and a variance of

$$\sigma^2 = 2\delta\tau N \frac{v_{\rm p}}{V_{\rm cell}} \tag{S12}$$

where V_{cell} is the volume per spatial grid point. The deterministic drift terms are given by

$$\Lambda_{-}(\mathbf{r}) = \frac{v_{\rm p}}{k_B T} \frac{\delta H[w]}{\delta w_{-}(\mathbf{r})} = \phi_{-}(\mathbf{r}) + \frac{2w_{-}(\mathbf{r})}{\chi N}$$
(S13)

$$\Lambda_{+}(\mathbf{r}) = \frac{v_{\mathrm{p}}}{k_{B}T} \frac{\delta H[w]}{\delta w_{+}(\mathbf{r})} = \phi_{+}(\mathbf{r}) - 1 - \frac{2w_{+}(\mathbf{r})}{(\chi + 2\zeta)N}$$
(S14)

where

$$\phi_{\pm}(\mathbf{r}) = \phi_A(\mathbf{r}) \pm \phi_B(\mathbf{r}) \tag{S15}$$

Here, $\phi_i(\mathbf{r})$ is a complex-valued generalization of the volume fraction of $i \in \{A, B\}$ monomers in the ideal gas reference system. In the canonical ensemble,

$$\phi_i(\mathbf{r}) = -V \frac{\delta \ln Q[w]}{\delta w_i(\mathbf{r})}$$
 (Canonical) (S16)

and in the grand-canonical ensemble,

$$\phi_i(\mathbf{r}) = -V e^{\mu/k_B T} \frac{\delta Q[w]}{\delta w_i(\mathbf{r})} \qquad \text{(Grand canonical)}$$
 (S17)

For a system with an analytic, translationally-invariant Hamiltonian, H[w], the Fokker-Planck operator corresponding to the CL eqs S10 and S11 will be invariant under generalized translations, i.e., under rigid translations of the w field configuration by any complex displacement. This is because the $\Lambda_{\pm}(\mathbf{r})$ terms (i.e., deterministic forces) are expressed as functional derivatives of H[w], and therefore they also undergo generalized translations. Furthermore, the random forces are chosen independently at each grid point from the same Gaussian distribution, and therefore the coefficients of the diffusive terms in the Fokker-Planck operator are independent of position and thus unaffected by generalized translations.

Demonstrating Analyticity

In the polymer field theory (before the complexification of the fields), the ensemble average of an observable O[w] is defined as a ratio of contour integrals,

$$\langle O[w] \rangle = \frac{\int O[w] P_c[w] \mathcal{D}w}{\int P_c[w] \mathcal{D}w}$$
 (S18)

For AB-type systems, $w_{-}(\mathbf{r})$ is real and $w_{+}(\mathbf{r})$ is imaginary along the contour. The theory underlying the CL-FTS method attempts to show that this average is equal to the time-average of O[w] generated by the CL sampling process in the limit of infinite time (i.e., $\tau \to \infty$). ^{4,5} Specifically, Gausterer and Lee^{6,7} have concluded that if the CL process is ergodic (i.e., if averages generated by CL sampling converge to unique limits and the associated probability distribution, P[w], converges to a unique steady-state solution) and if $P_c[w]$ and O[w] are both entire analytic functions (i.e., are differentiable throughout the complex function space, without branch cuts or poles), then the CL time average of O[w] will converge to that of eq S18. Note that the reasoning used to reach this conclusion relies on the analyticity of $P_c[w]$ rather than H[w]. This distinction is relevant because we find below that, in the canonical ensemble, $P_c[w]$ is entire while H[w] is not.

Properties of Analyticity. We use the notation A[w] to indicate that A is a complexvalued functional of w. Suppose δA is the infinitesimal perturbation of A[w] induced by a perturbation δw of field w, defined by specifying an infinitesimal perturbation for each field component, $\delta w_i(\mathbf{r})$, for i = 1, ..., M. If $c\delta A$ equals the perturbation of A induced by a perturbation $c\delta w$ for any finite complex constant c, then A[w] is an analytic functional. Using this property, one can easily confirm the following theorems:

(I) If A[w] is equal to a sum

$$A[w] = bB[w] + cC[w] \tag{S19}$$

in which B[w] and C[w] are analytic functionals while b and c are complex constants,

then A[w] is also an analytic functional.

(II) If A[w] is equal to a product

$$A[w] = B[w]C[w] \tag{S20}$$

of two analytic functionals B[w] and C[w], then A[w] is again analytic.

(III) If A[w] is defined as an integral

$$A[w] = \int f(w(\mathbf{r})) d\mathbf{r}$$
 (S21)

in which $f(w(\mathbf{r})) = f(w_1(\mathbf{r}), \dots, w_M(\mathbf{r}))$ is a scalar complex-valued analytic function of the multi-component field, and the integral is taken over all \mathbf{r} within a periodic domain, then A[w] is an analytic functional.

(IV) If A[w] is defined as

$$A[w] = f(B[w]) \tag{S22}$$

where f(z) is an analytic complex-valued function of a complex argument z and B[w] is an analytic functional of w, then A[w] is an analytic functional of w.

We will also need the fact that a power (monomial) function $f(z) = z^p$ with a non-negative integer exponent is analytic in z throughout the complex plane, as is any sum of such monomials (i.e., any polynomial), and as is the exponential function $f(z) = e^{cz}$ with any complex constant c.

Generalized Boltzmann Weight. The generalized Boltzmann weight can be expressed, using eq S4, as

$$P_{c}[w] = Z_{id}[w] e^{-H_{f}[w]/k_{B}T}$$
 (S23)

Referring to eq S5, $H_f[w]$ is a spatial integral of a quadratic polynomial in the fields, and is thus entire by theorem III. It follows that $e^{-H_f[w]/k_BT}$ is also entire by theorem IV. Expressions

for $Z_{id}[w]$ are given in eqs S8 and S9 for the canonical and grand-canonical ensembles, respectively. In both cases, $Z_{id}[w]$ is an analytic function of Q[w], and therefore, by theorem IV, $Z_{id}[w]$ is entire if Q[w] is entire. From this, we conclude from theorem II that $P_{c}[w]$ will be entire if Q[w] is entire.

Ideal Gas of Continuous Chains. Our SCFT calculations were performed using the standard Gaussian chain model (GCM),⁸ where the system is treated as an incompressible melt ($\zeta \to \infty$) of continuous Gaussian chains. The single-chain partition function for a continuous chain is given by

$$Q[w] = \frac{1}{V} \int q(\mathbf{r}, 1) d\mathbf{r}$$
 (S24)

where $q(\mathbf{r}, s)$ is the solution of the modified diffusion equation (MDE)

$$\frac{\partial q(\mathbf{r}, s)}{\partial s} = \left[\frac{a^2 N}{6} \nabla^2 - w_{\alpha(s)}(\mathbf{r}) \right] q(\mathbf{r}, s)$$
 (S25)

with an initial condition $q(\mathbf{r}, 0) = 1$. Here, $s \in [0, 1]$ is a contour coordinate along the chain and $\alpha(s)$ denotes the monomer type at position s. For a diblock copolymer, $\alpha(s) = A$ if $s \in [0, f]$ and $\alpha(s) = B$ if $s \in [f, 1]$. For simplicity, eq S25 assumes that the A and B monomers have an equal statistical segment length, denoted by a.

By theorem III, it follows that Q[w] will be analytic provided $q(\mathbf{r}, s)$ is analytic. Thus, we need to consider how the solution to the MDE changes under an infinitesimal change in w. Suppose that $q^{(0)}(\mathbf{r}, s)$ is the solution of the MDE in the presence of a multi-component field, $w_i^{(0)}(\mathbf{r})$, such that

$$\left[\frac{\partial}{\partial s} - \frac{a^2 N}{6} \nabla^2 + w_{\alpha(s)}^{(0)}(\mathbf{r})\right] q^{(0)}(\mathbf{r}, s) = 0$$
 (S26)

Let $q(\mathbf{r}, s)$ denote the solution of the MDE for infinitesimal perturbations of the field com-

ponents, $w_i(\mathbf{r})$, such that

$$w_i(\mathbf{r}) = w_i^{(0)}(\mathbf{r}) + \delta w_i(\mathbf{r}) \tag{S27}$$

$$q(\mathbf{r}, s) = q^{(0)}(\mathbf{r}, s) + \delta q(\mathbf{r}, s)$$
(S28)

Substituting these definitions into the MDE and retaining terms up to first order in δw , we find that the perturbation δq induced by the perturbation δw must satisfy

$$\left[\frac{\partial}{\partial s} - \frac{a^2 N}{6} \nabla^2 + w_{\alpha(s)}^{(0)}(\mathbf{r})\right] \delta q(\mathbf{r}, s) = q^{(0)}(\mathbf{r}, s) \delta w_{\alpha(s)}(\mathbf{r})$$
(S29)

Notice that eq S29 is linear in both δq and δw . Therefore, if δq is the change in q induced by δw , then $c\delta q$ is the change in q induced by $c\delta w$, where c is any finite complex constant. This observation demonstrates that $q(\mathbf{r}, s)$ is an analytic functional of the fields.

Ideal Gas of Discrete Chains. Our CL-FTSs treated the system as a compressible melt ($\zeta = 1$) of discrete Gaussian chains with N = 90 monomers per chain, labeled i = 1, 2, 3, ..., N. In this model,

$$Q[w] = \frac{1}{V} \int q_N(\mathbf{r}) d\mathbf{r}$$
 (S30)

where $q_N(\mathbf{r})$ is obtained by iterating the convolution integral

$$q_{i+1}(\mathbf{r}) = e^{w_{\alpha_i}(\mathbf{r})/N} \left(\frac{3}{2\pi a^2}\right)^{3/2} \int q_i(\mathbf{r} - \mathbf{R}) e^{-3R^2/2a^2} d\mathbf{R}$$
 (S31)

starting from $q_1(\mathbf{r}) = e^{-w_{\alpha_1}(\mathbf{r})/N}$. Here, α_i denotes the type (A or B) of monomer *i*. In this case, the analyticity of $q_i(\mathbf{r})$ follows from the repeated application of theorems II and III. The analyticity of Q[w] is then a direct result of theorem III.

Note that, as mentioned in the main paper, the CL-FTSs can be mapped onto the standard GCM used for the SCFT calculations. This is done by performing the CL-FTSs with χ replaced by χ_b in eq S5 and a replaced by a_b in eq S31. Effective values for χ and a corresponding to the GCM are then calculated as described in ref 9.

Analytic Properties of the Hamiltonian. We now consider the analyticity of the Hamiltonian, H[w]. Although $P_c[w]$, defined in eq S3, is entire if H[w] is since $f(z) = e^{cz}$ is an analytic function, the converse is not necessarily true. Referring to the expression for H[w] in eq S4, the issue is whether $\ln Z_{id}[w]$ is also entire, since we have already established that $H_f[w]$ is entire. In the canonical ensemble,

$$\ln Z_{\rm id} = n \ln(VQ[w]/v_{\rm p}) - \ln(n!) \qquad \text{(Canonical)}$$

The presence of the natural logarithm requires the introduction of a branch cut, across which the imaginary part of $\ln Q[w]$ and thus H[w] is discontinuous. Therefore, H[w] will not be entire, even though Q[w] and $P_{c}[w]$ are. On the other hand, in the grand-canonical ensemble,

$$\ln Z_{\rm id} = e^{\mu/k_B T} V Q[w]/v_{\rm p} \qquad \text{(Grand canonical)} \tag{S33}$$

is entire given that it is simply proportional to Q[w]. Hence, H[w] will be entire in the grand-canonical ensemble.

For simplicity, the associated article assumed that H[w] is an analytic functional for all w. Clearly, this is not true in the canonical ensemble, because of the branch cut required to render $\ln Q[w]$ single-valued. We also note, however, that the above logic underlying the use of the CL method to evaluate ensemble averages of analytic observables, O[w], only seems to require that $P_c[w]$ is entire, which is true in both ensembles. For instance, the deterministic drift terms in the CL eqs S13 and S14 can be expressed as

$$\Lambda_{\pm}(\mathbf{r}) = -\frac{v_{\rm p}}{P_c[w]} \frac{\delta P_c[w]}{\delta w_{\pm}(\mathbf{r})}$$
(S34)

which ensures that they are analytic and continuous everywhere that $P_c[w] \neq 0$. The arguments given in the accompanying article about the consequences of the analyticity and

translational invariance, though phrased as statements about H[w], could all have been equally well phrased as statements about $P_{c}[w]$, without changing any of our conclusions. We thus believe that the justification for CL averages of analytic observables is valid in either the canonical or grand-canonical ensemble.

The fact that H[w] requires a branch cut in the canonical ensemble does, however, imply that treating H[w] as an observable is potentially problematic. If the value of Q[w] during a CL-FTS in the canonical ensemble were to cross the branch cut of the logarithmic function, which is generally placed along the negative part of the real axis, then the imaginary part of $\ln Q[w]$, and hence of $H[w]/nk_BT$, would change discontinuously by $\pm 2\pi$. However, the fact that Q[w] is analytic and translationally invariant implies that it has the same positive real value for the entire family of complex SCFT solutions, about which CL-FTSs fluctuate. Provided that the fields do not fluctuate too far from these saddle-points, which is the case in our CL-FTSs, Q[w] will remain far from the branch cut. Indeed, Figure 5b in the main paper shows no evidence of a discontinuity in $Im[H/nk_BT]$, at least while the CL-FTS is behaving properly. Note that CL simulations of other systems with logarithmic terms have encountered convergence problems when the argument of the logarithm (i.e., Q[w] in our case) winds around the origin, 10,11 but this too is not a problem in our CL-FTSs given that Q[w] does not generally fluctuate far from the SCFT value.

SCFT Results

Here, we provide additional SCFT results for diblock copolymer melts to supplement the ones in the main paper. In particular, Figure S1 provides analogous plots to Figure 2 for the lamellar phase, but at a substantially stronger segregation. The top part of Figure S2 shows the fields of the real saddle-point for the cylindrical phase, while the bottom part shows the complex saddle-point resulting from an imaginary translation in the x direction. Figure S3 then shows the complex saddle-point resulting from an imaginary translation in

the y direction.

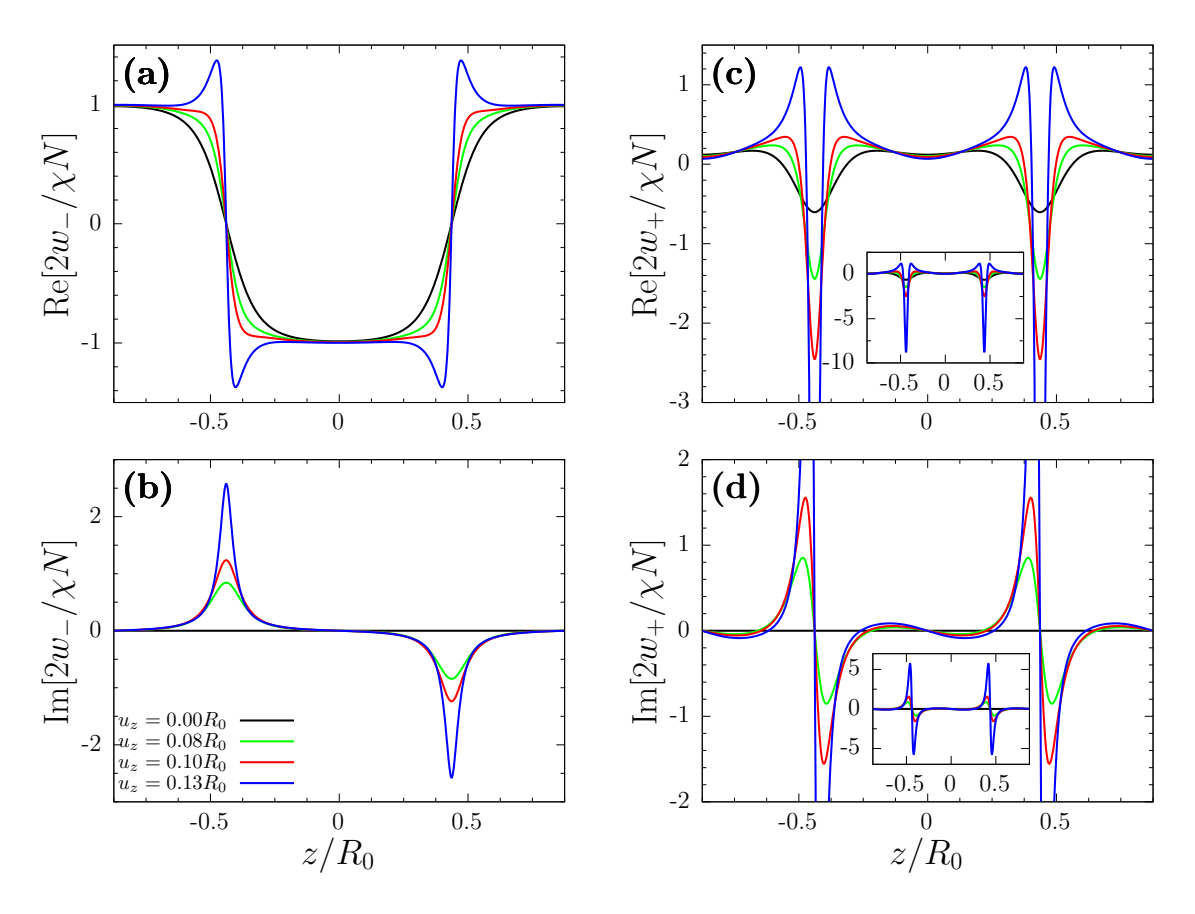


Figure S1: Complex saddle-point solution for an AB diblock copolymer lamellar phase with f=0.5 and $\chi N=25$, plotted for increasing imaginary distance, u_z , from the real saddle-point. The real and imaginary parts of $w_-(z)$ are shown in plots (a) and (b), respectively, and the real and imaginary parts of $w_+(z)$ are shown in plots (c) and (d), respectively. The insets show a reduced scale to capture the large field values for $u_z=0.13R_0$.

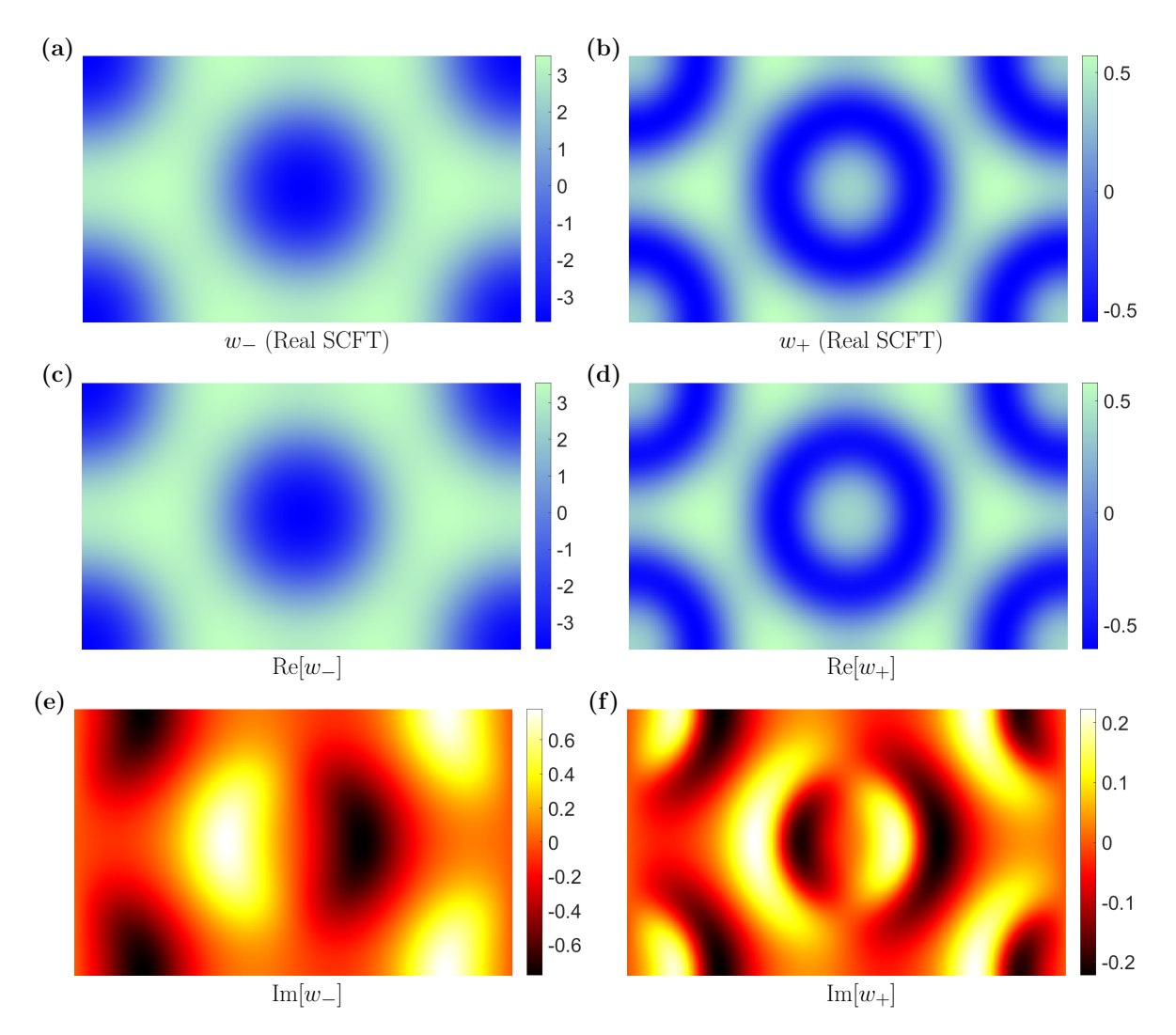


Figure S2: Real SCFT solution for an AB diblock copolymer cylindrical phase with f=0.4 and $\chi N=12$. The fields $w_{-}(\mathbf{r})$ and $w_{+}(\mathbf{r})$ are plotted in (a) and (b), respectively. Complex SCFT solution resulting from an imaginary displacement of $\mathbf{u}=0.05R_0\hat{\mathbf{i}}$. The real parts of $w_{-}(\mathbf{r})$ and $w_{+}(\mathbf{r})$ are shown in plots (c) and (d), respectively, and the imaginary parts are shown in plots (e) and (f), respectively. The size of each image is $2.70R_0 \times 1.56R_0$.

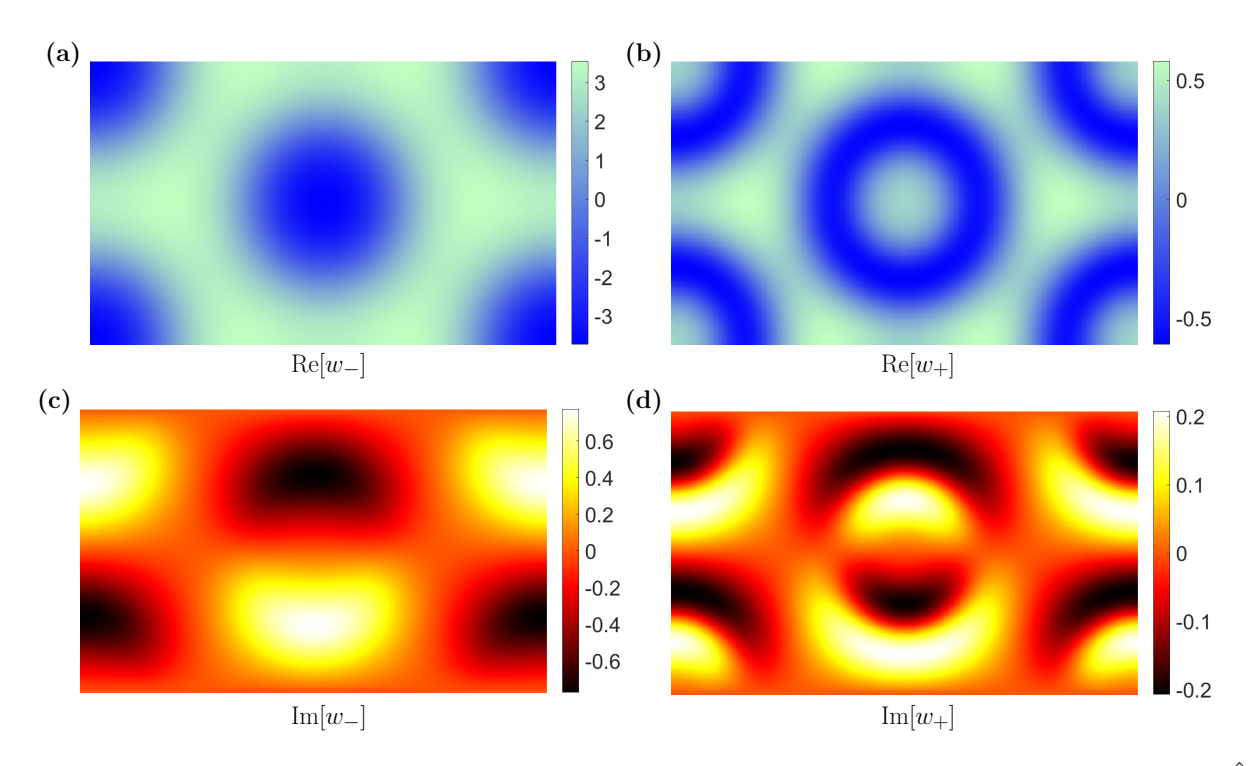


Figure S3: Complex SCFT solution resulting from an imaginary displacement of $\mathbf{u} = 0.05 R_0 \hat{\mathbf{j}}$ from the real SCFT solution in Figure S2. The real parts of $w_{-}(\mathbf{r})$ and $w_{+}(\mathbf{r})$ are shown in plots (a) and (b), respectively, and the imaginary parts are shown in plots (c) and (d), respectively. The size of each figure is $2.70R_0 \times 1.56R_0$.

CL-FTS Results

Figure S4 shows CL-FTS results for the lamellar phase at different points along the line of complex saddle-points. The position, u_z , is controlled by adjusting the C_z parameter in eq 20 of the main paper (see Table I). The top graph confirms that translation cooling holds the imaginary amplitude of $w_-(z)$, defined in eq 11 of the main paper, relatively constant. Note that for $C_z = 1.8$ (gray curve), the CL-FTS crashed at $\tau N \approx 2.1 \times 10^5$ due to the formation of a hot spot. The bottom graph shows that Im[H] maintains a Gaussian distribution with a mean of zero. The width of the distribution does, however, increase noticeably for $C_z \gtrsim 1$ presumably due to hot-spot-like fluctuations. Consistent with this, the Gaussian distribution develops tails for $C_z \gtrsim 1.5$.

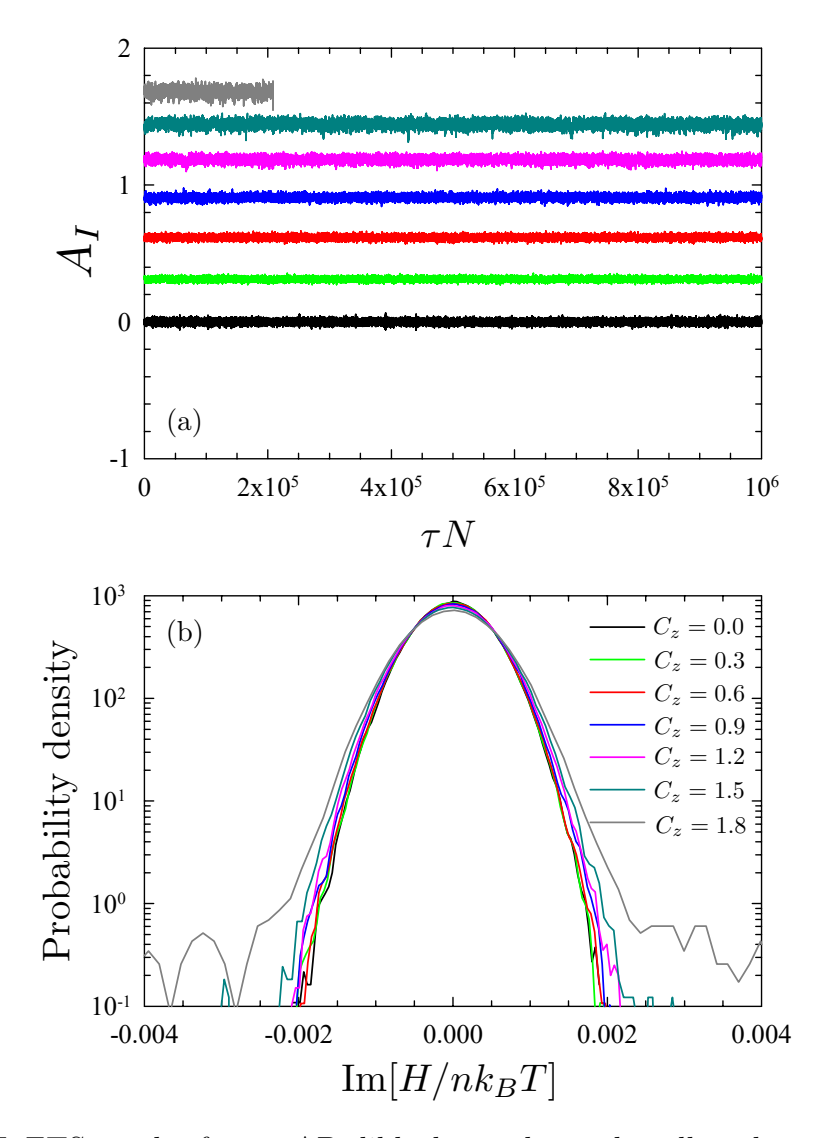


Figure S4: CL-FTS results for an AB diblock copolymer lamellar phase with f=0.5 and $\chi N=12$, where the C_z for translation cooling is adjusted to hold the system at different positions, u_z , along the line of complex saddle-points. Amplitudes of the imaginary part of $w_{-}(\mathbf{r})$ are plotted as a function of simulation time in (a) and histograms of the imaginary part of the Hamiltonian are plotted in (b).

References

(1) Delaney, K. T.; Fredrickson, G. H. Recent Developments in Fully Fluctuating Field-Theoretic Simulations of Polymer Melts and Solutions. J. Phys. Chem. B 2016, 120, 7615–7634.

- (2) Matsen, M. W.; Willis, J. D.; Beardsley, T. M. Accurate Universal Predictions for Block Copolymer Melts Using Field-Theoretic Simulations. *Macromolecules* 2024, 57, 4312–4322.
- (3) Fredrickson, G. H.; Ganesan, V.; Drolet, F. Field-Theoretic Computer Simulation Methods for Polymers and Complex Fluids. *Macromolecules* **2002**, *35*, 16–39.
- (4) Fredrickson, G. H. *The Equilibrium Theory of Inhomogeneous Polymers*; Oxford University Press: Oxford, 2006.
- (5) Fredrickson, G. H.; Delaney, K. T. Field-Theoretic Simulations in Soft Matter and Quantum Fluids; Oxford University Press: Oxford, 2023.
- (6) Gausterer, H.; Lee, S. The Mechanism of Complex Langevin Simulations. *J. Stat. Phys.* **1993**, 73, 147–157.
- (7) Lee, S. The Convergence of Complex Langevin Simulations. *J. Nucl. Phys.* **1994**, *413*, 827–848.
- (8) Matsen, M. W. The standard Gaussian model for block copolymer melts. *J. Phys.: Condens. Matter* **2002**, *14*, R21–R47.
- (9) Matsen, M. W.; Willis, J. D.; Beardsley, T. M. Accurate Universal Predictions for Block Copolymer Melts Using Field-Theoretic Simulations. *Macromolecules* 2024, 57, 4312–4322.
- (10) Mollgaard, A.; Splittorff, K. Complex Langevin dynamics for chiral random matrix theory. *Phys. Rev. D* **2013**, *88*, 116007.
- (11) Mollgaard, A.; Splittorff, K. Full simulation of chiral random matrix theory at nonzero chemical potential by complex Langevin. *Phys. Rev. D* **2015**, *91*, 036007.